School on Synchrotron and Free-Electron-Laser Methods for Multidisciplinary Applications

7-18 May 2018
Trieste, Italy

ICTP
The Abdus Salam
International Centre for Theoretical Physics
www.ictp.it
Trieste, Italy

IAEA

UNIVERSITAS STUDIORUM ATHESINA

Basic Aspects of x-ray crystallography and powder diffraction

-

Diffraction from nanocrystalline materials

Paolo.Scardi@unitn.it

Special thanks to: Luca Rebuffi & Binayak Mukherjee

PRESENTATION OUTLINE

PART I May 10, 9:00 – 10:30

- Powder diffraction: basic elements
- Nanocrystalline & severely deformed materials

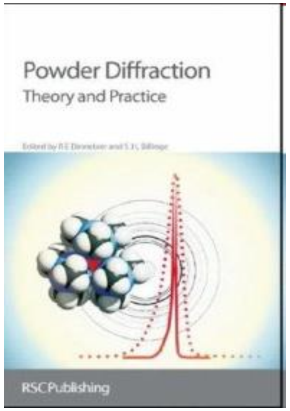
Powder Diffraction
Theory and Practice
Edited by R.E. Dinnebier and S.J.L. Billinge
RSC Publishing

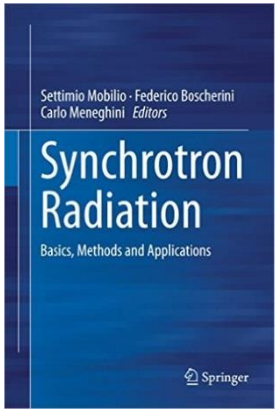
Settimio Mobilio · Federico Boscherini
Carlo Meneghini *Editors*
Synchrotron Radiation
Basics, Methods and Applications
Springer

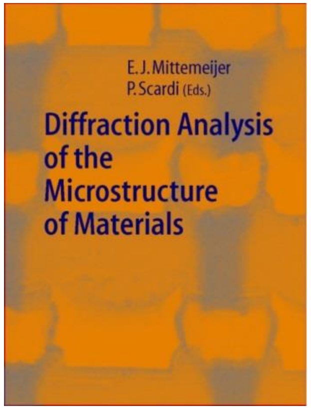
E.J. Mittemeijer
P. Scardi (Eds.)
Diffraction Analysis of the Microstructure of Materials

PART II May 10, 17:00 – 18:30

- Computer lab:
  hands-on session with TOPAS

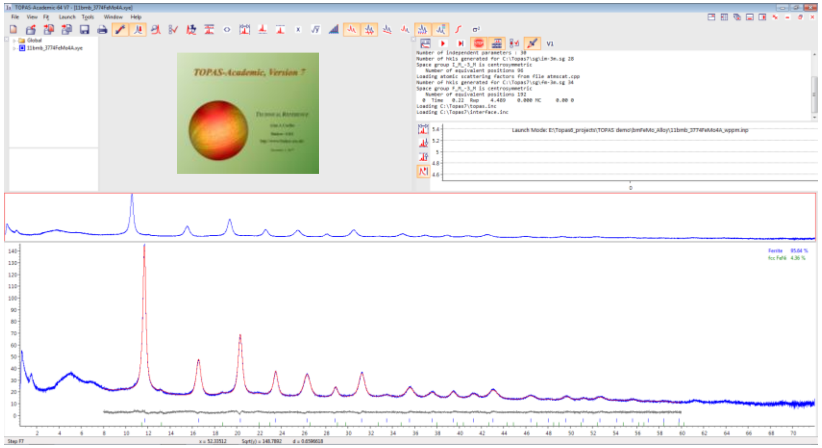

1912 - THE DISCOVERY OF X-RAY DIFFRACTION

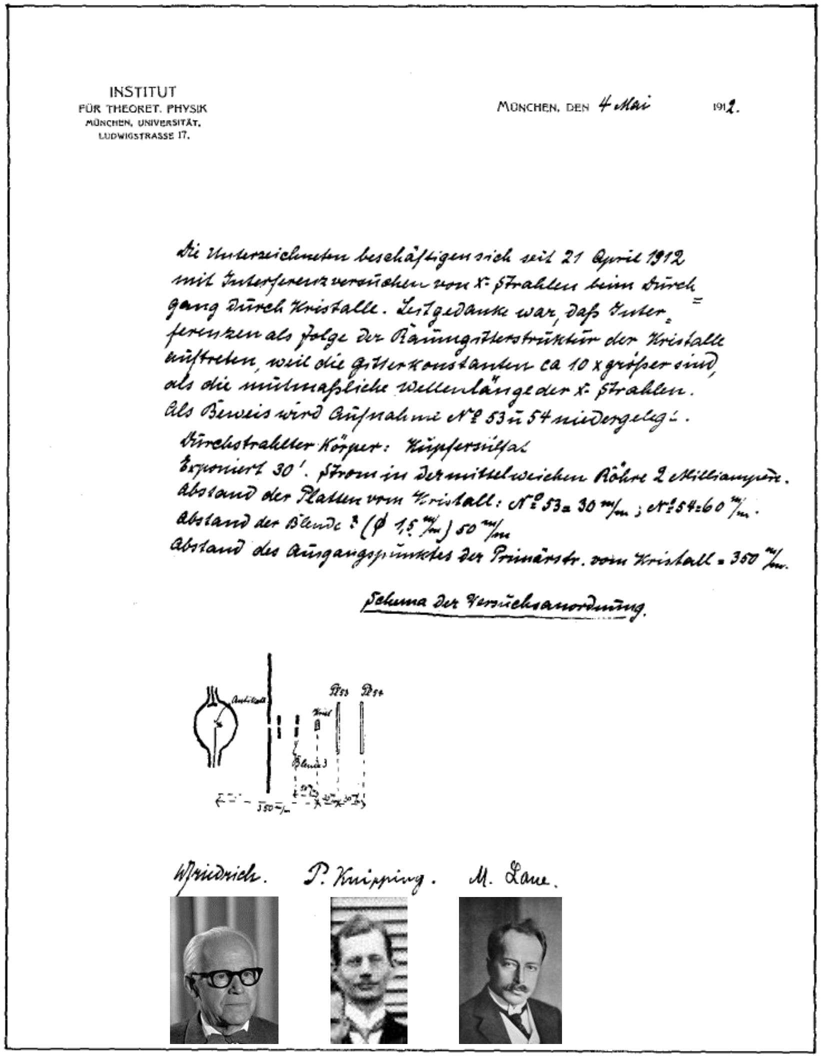

INSTITUT
FÜR THEORET. PHYSIK
MÜNCHEN, UNIVERSITÄT,
LUDWIGSTRASSE 17.

MÜNCHEN, DEN 4 Mai 1912.

Die Unterzeichneten beschäftigen sich seit 21 April 1912 mit Interferenzversuchen von X-Strahlen beim Durchgang durch Kristalle. Leitgedanke war, daß Interferenzen als Folge der Raumgitterstruktur der Kristalle auftreten, weil die Gitterkonstanten ca 10 x größer sind, als die mutmaßliche Wellenlänge der X-Strahlen.
Als Beweis wird Aufnahme N° 53 u 54 niedergelegt.
Durchstrahlter Körper: Kupfersulfat
Exponiert 30'. Strom in der mittelweichen Röhre 2 Milliampère.
Abstand der Platten vom Kristall: N° 53 = 30 m/m ; N° 54 = 60 m/m.
Abstand der Blende 3 (ϕ 1,5 m/m) 50 m/m
Abstand des Ausgangspunktes der Primärstr. vom Kristall = 350 m/m.

Schema der Versuchsanordnung.

W. Friedrich. P. Knipping. M. Laue.

Fig. 1. Sealed note deposited by A. Sommerfeld with the Bavarian Academy of Sciences on 4 May 1912 in order to protect Friedrich, Knipping, and Laue's priority in the discovery of the diffraction of X-rays by crystals. (Photo Deutsches Museum München, Lichtbildnummer: 30497)

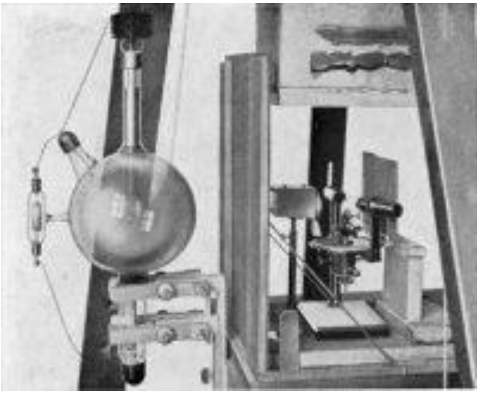

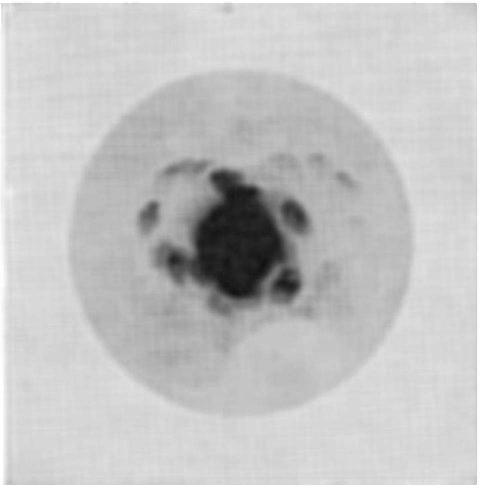

copper sulfate (triclinic)
random orientation

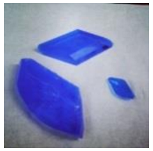

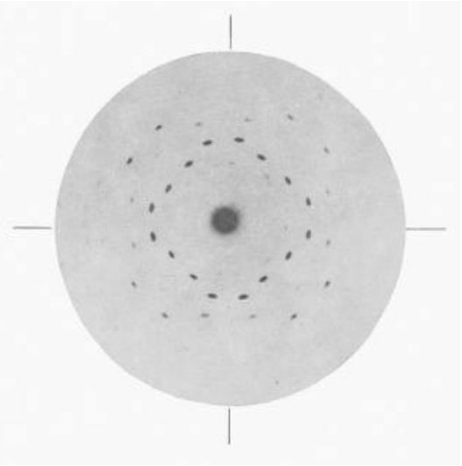

zinc blende (cubic)

1916 - FROM SINGLE-CRYSTAL TO POWDER DIFFRACTION

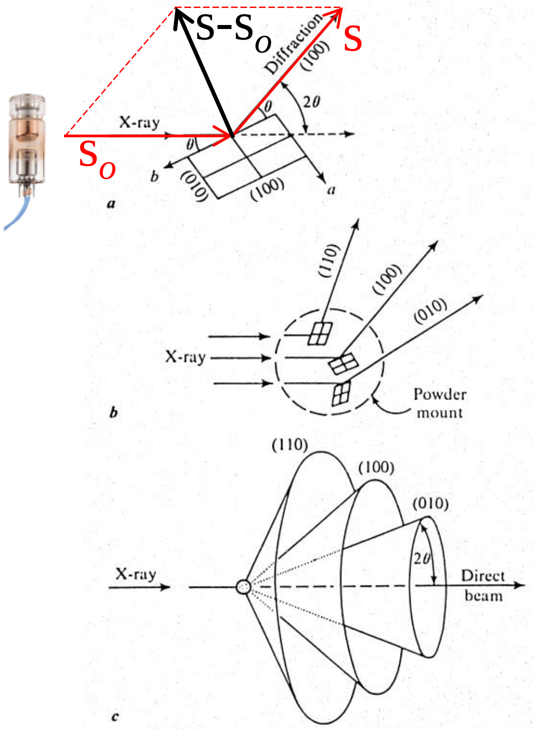

FIGURE 10.11 Diffraction of monochromatic x-rays from (a) a single crystal and (b) an aggregate of small mineral fragments. (c) Diffraction cones produced by the powder method.

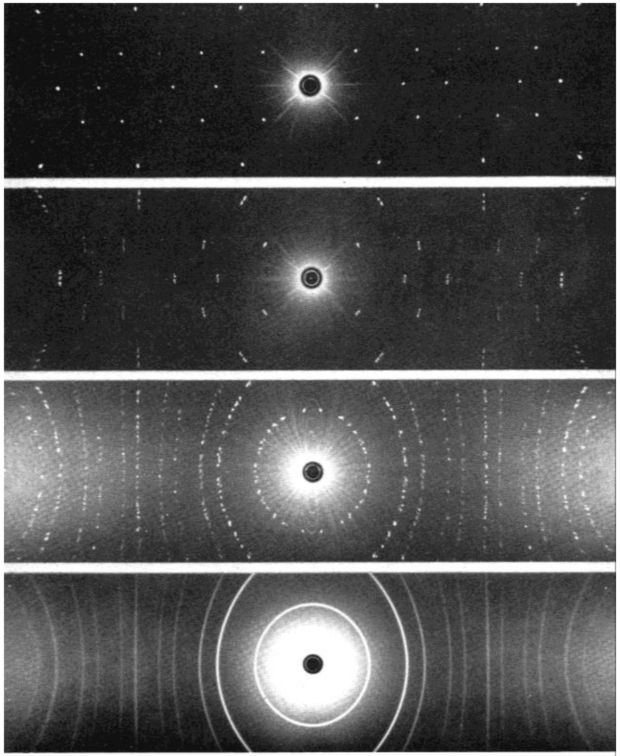

(From top to bottom). Fig. 197: Single-crystal rotation photograph of fluorite [100] vertical: Fig. 198: Single-crystal rotation photograph of fluorite [100] 2° to vertical: Fig. 199: X-ray photograph of five randomly oriented crystals of fluorite: Fig. 200: Powder photograph of fluorite.

Laue diffraction conditions

$$\mathbf{a}\cdot(\mathbf{s}-\mathbf{s}_o)=h\lambda$$

$$\mathbf{b}\cdot(\mathbf{s}-\mathbf{s}_o)=k\lambda$$

$$\mathbf{c}\cdot(\mathbf{s}-\mathbf{s}_o)=l\lambda$$

Bragg's law

$$2d(hkl)\sin\theta=\lambda$$

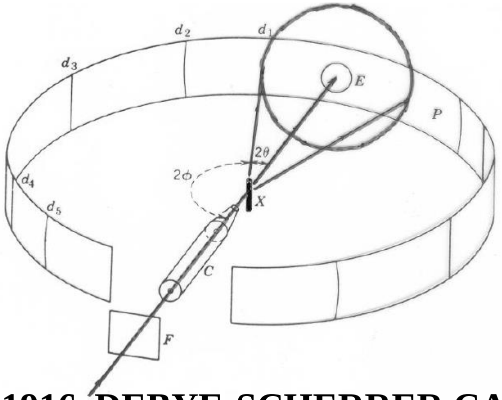

1916 DEBYE-SCHERRER CAMERA

BRAGG LAW

Interference of X-rays scattered by atomic planes

$$MP + PN = 2d_{hkl} \sin\theta_B = n\lambda$$

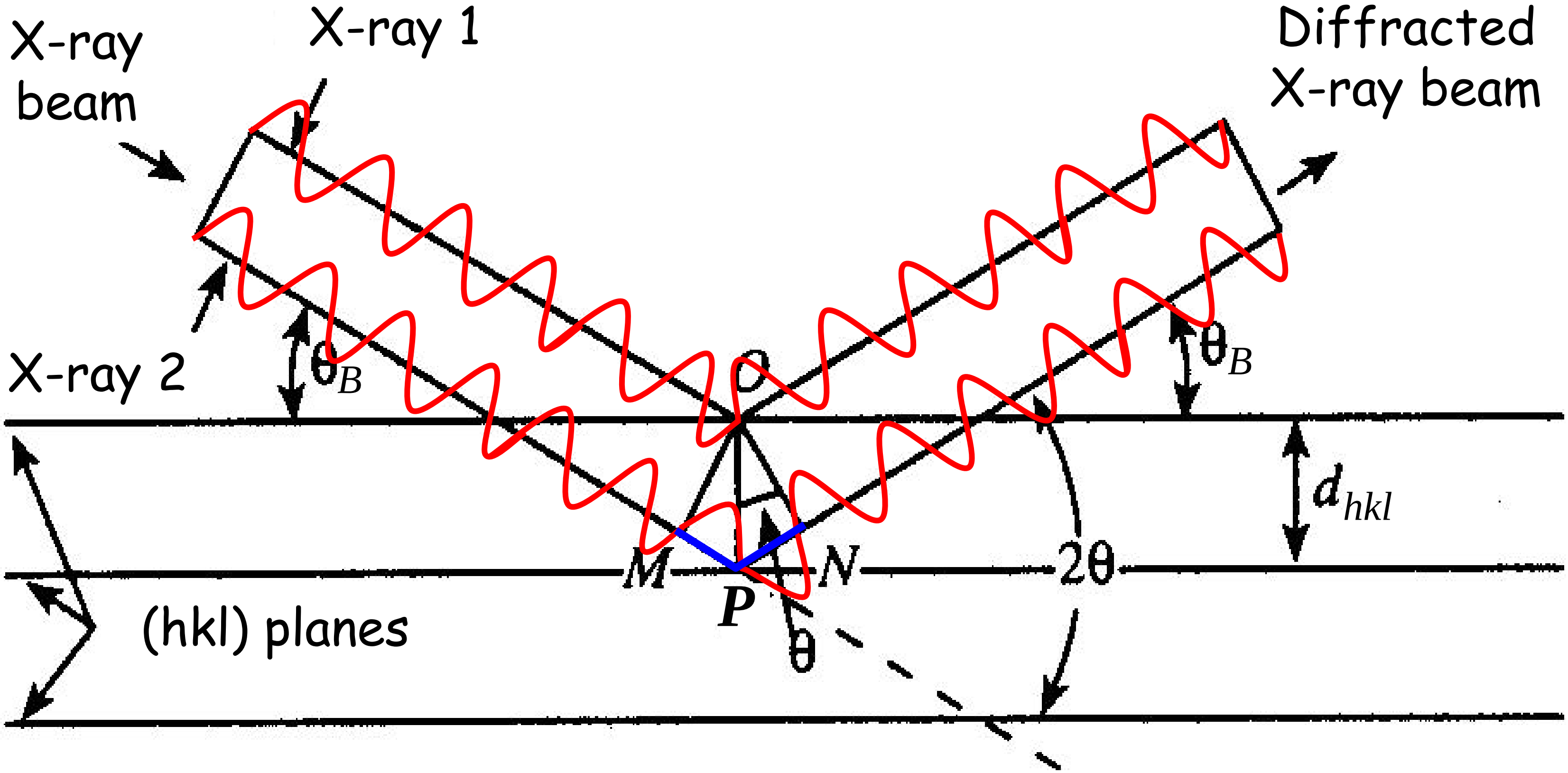

BRAGG LAW

Interference of X-rays scattered by atomic planes

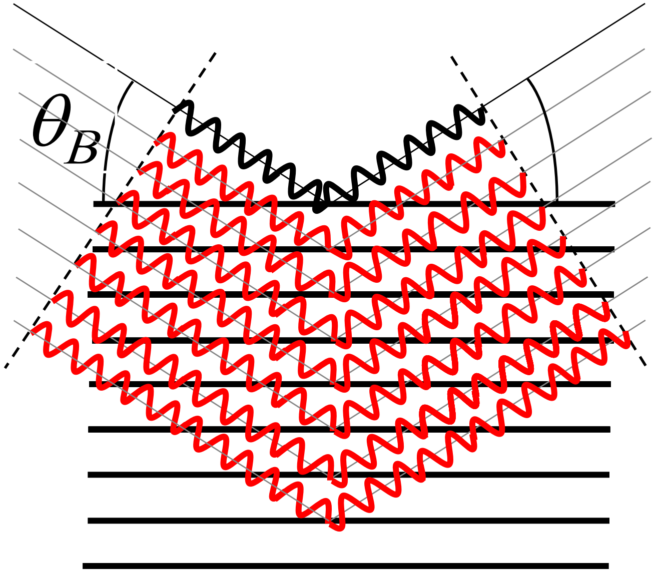

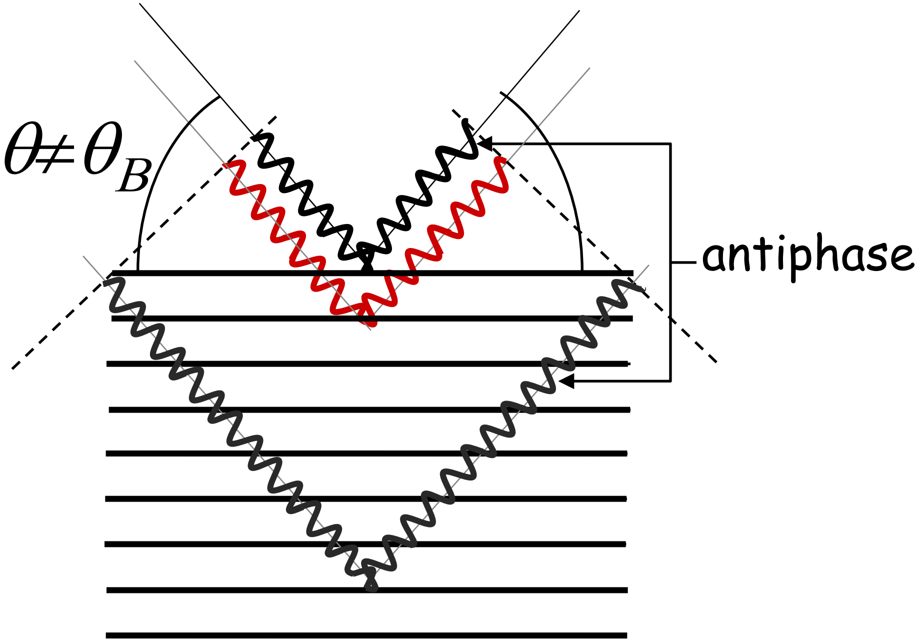

in Bragg condition:

all waves **in phase**

irrespective of depth
from the surface.

not in Bragg condition:

phase relations **change** with depth

at a certain depth, a reflected wave is in antiphase with the surface: the two waves cancel each- other

BRAGG LAW

Interference of X-rays scattered by atomic planes

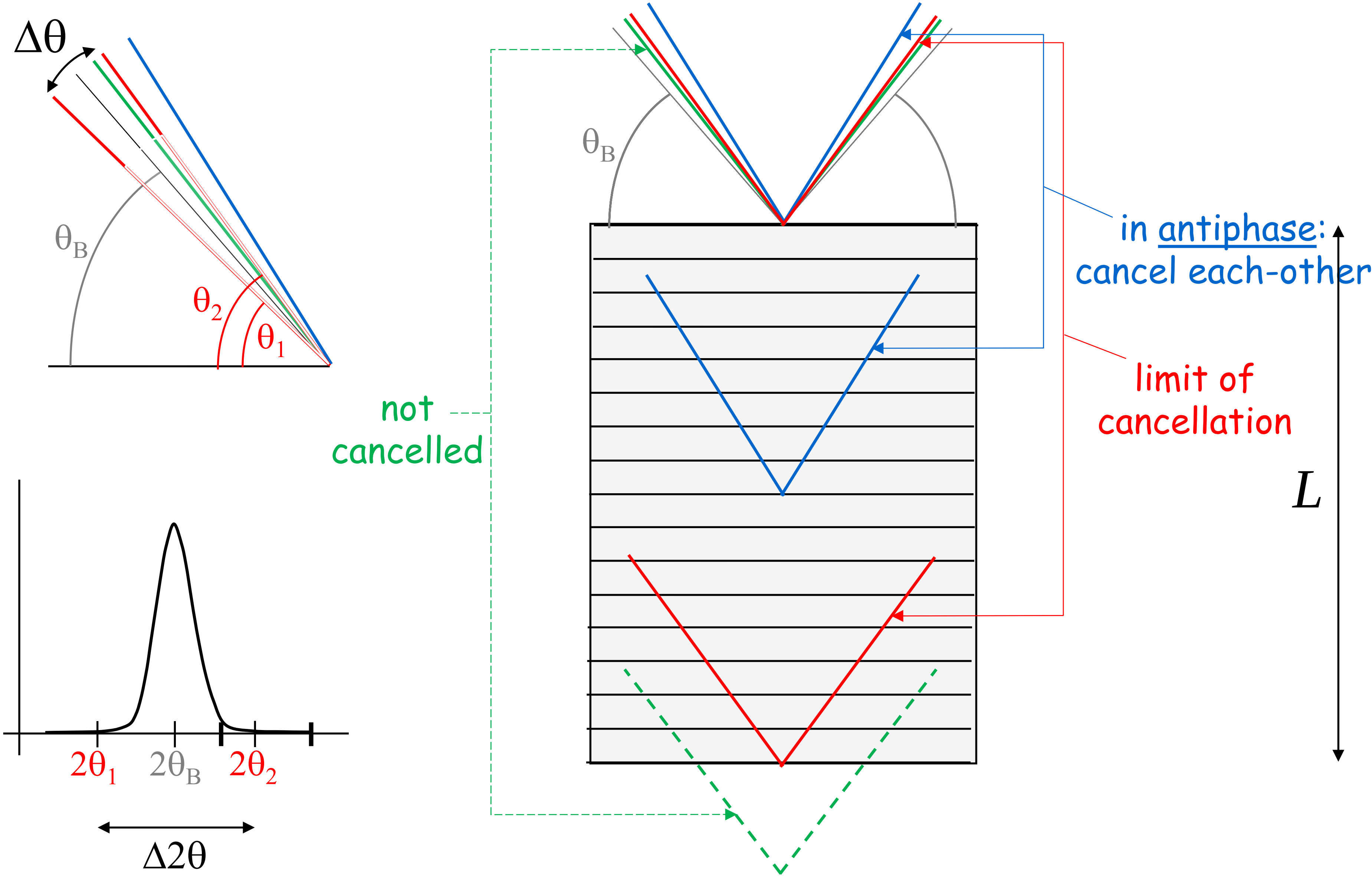

not cancelled

in antiphase: cancel each-other

limit of cancellation

SCHERRER EQUATION

Peak width is inversely proportional to the crystalline domain thickness

$$\Delta 2\theta \propto \frac{1}{L} = \frac{\lambda}{L\cos\theta_B}$$

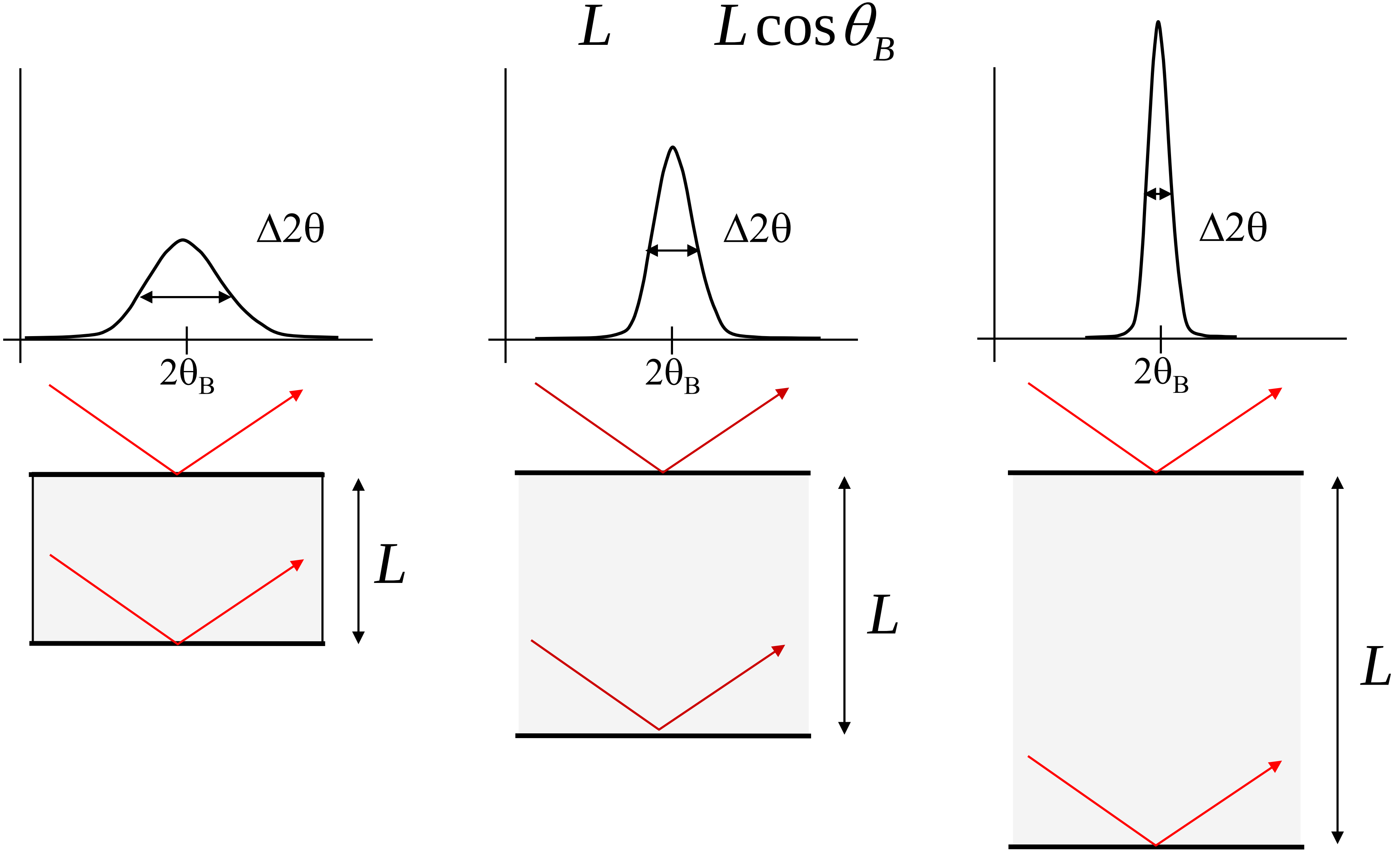

X-RAY DIFFRACTION (XRD) FROM SMALL CRYSTALS

MgO powder

J.T. Randall, The diffraction of X-rays and electrons by amorphous, solids, liquids, and gases, 1934

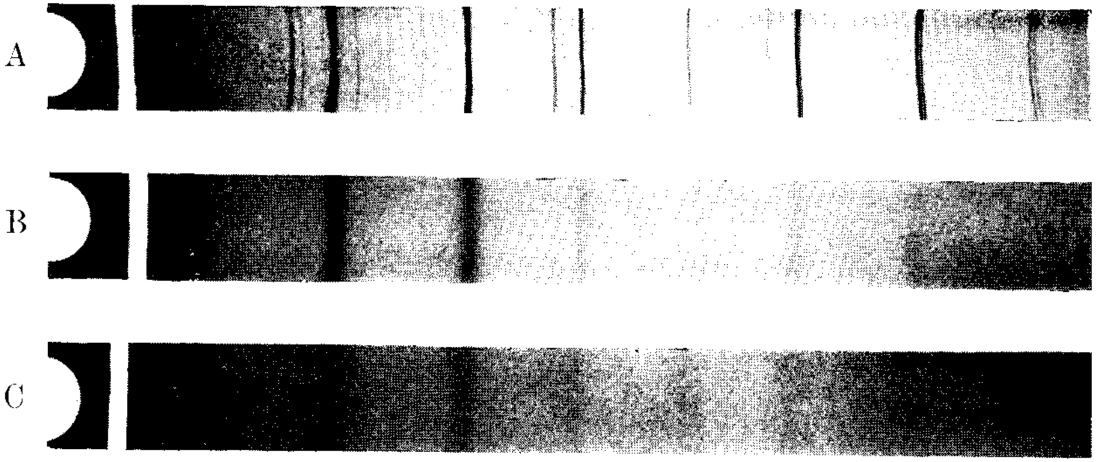

FIG. 31.—The effect of crystal size on line width for magnesium oxide. The uppermost photograph *A* has typically sharp lines. In the lower photographs *B* and *C* the lines have broadened considerably owing to reduction in size of the crystalline particles of oxide. The particles are here sufficiently small to prevent the resolution of the Cu-Kα doublet which can be clearly seen in photograph *A*. The specimens *A*, *B*, *C* were formed by the decomposition of $MgCO_3$ at successively lower temperatures.

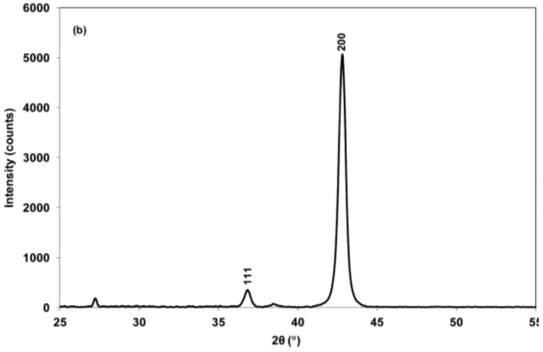

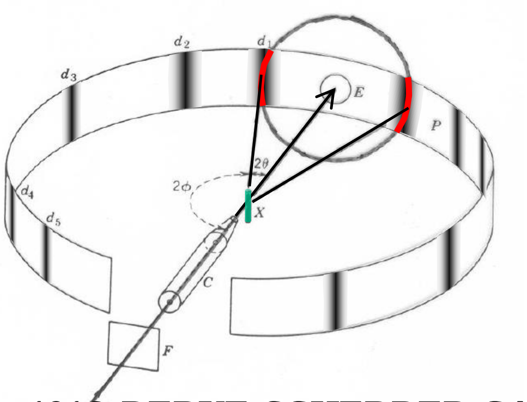

1916 DEBYE-SCHERRER CAMERA

XRD FROM SMALL CRYSTALS: SCHERRER EQUATION

Determination of the size and internal structure of colloid particles by means of x-rays

by

P. Scherrer.

Presented by P. Debye in the meeting of 26. Juli 1918.

… … … The theory provides for the half-value width ***h*** of the maximum defined in the known manner, which occurs at the angle ϑ to the incident X-ray beam, the value:

$$h = 2\sqrt{\frac{\ln 2}{\pi}} \cdot \frac{\lambda}{\Lambda} \cdot \frac{1}{\cos \vartheta/2}.$$

λ/Λ is the ratio of the wavelength of the monochromatic X-rays used to the edge of the crystal presumed to be cube-shaped

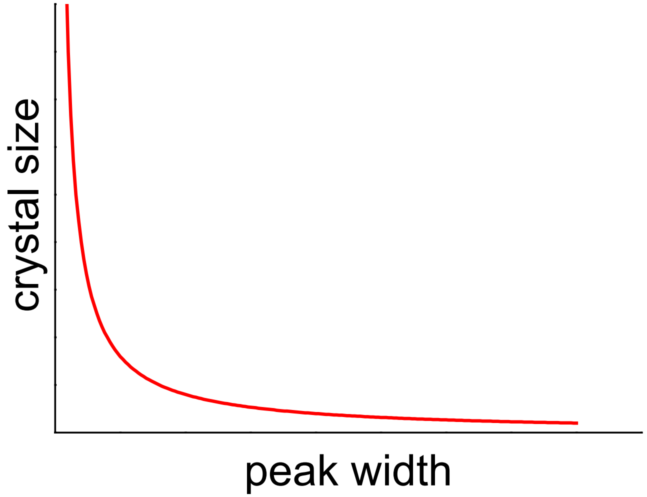

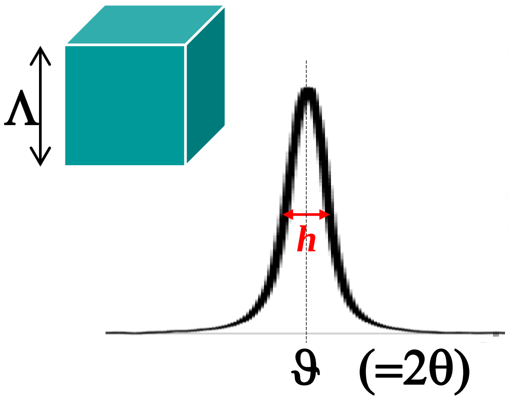

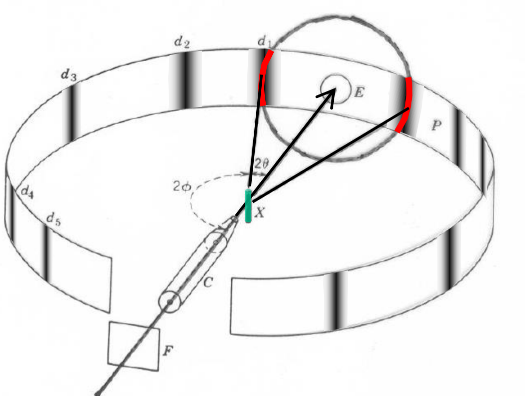

1916 DEBYE-SCHERRER CAMERA

PRACTICE: SCHERRER EQUATION

(220) peak of nanocrystalline CeO_2

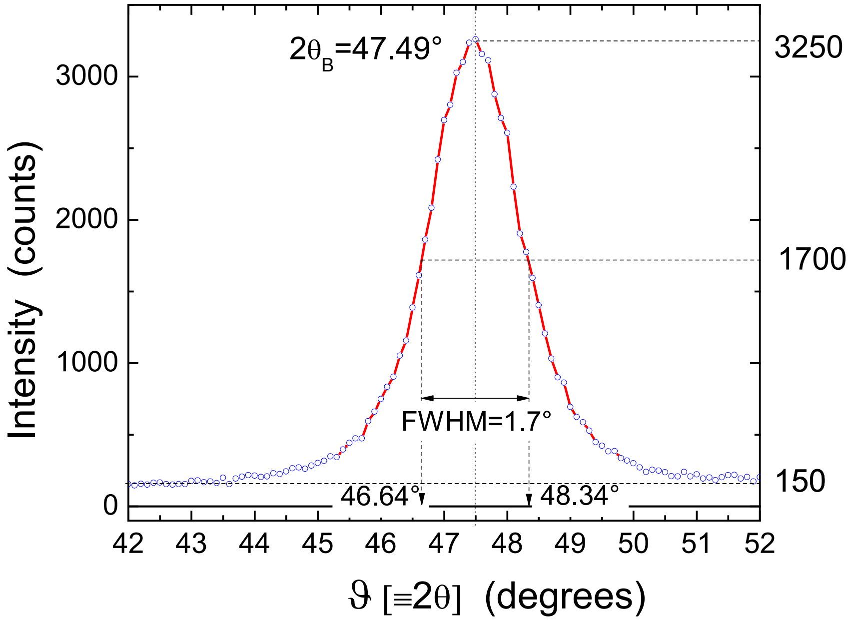

$\Lambda = ?$

$$h = 2\sqrt{\frac{\ln 2}{\pi}} \frac{\lambda}{\Lambda \cos\left(\vartheta_B / 2\right)}$$

Λ : *effective* crystalline domain size (in nm)

h : full width at half maximum (FWHM in radians)

λ = 0.15406 nm (X-ray wavelength)

LABORATORY vs SYNCHROTRON RADIATION XRD

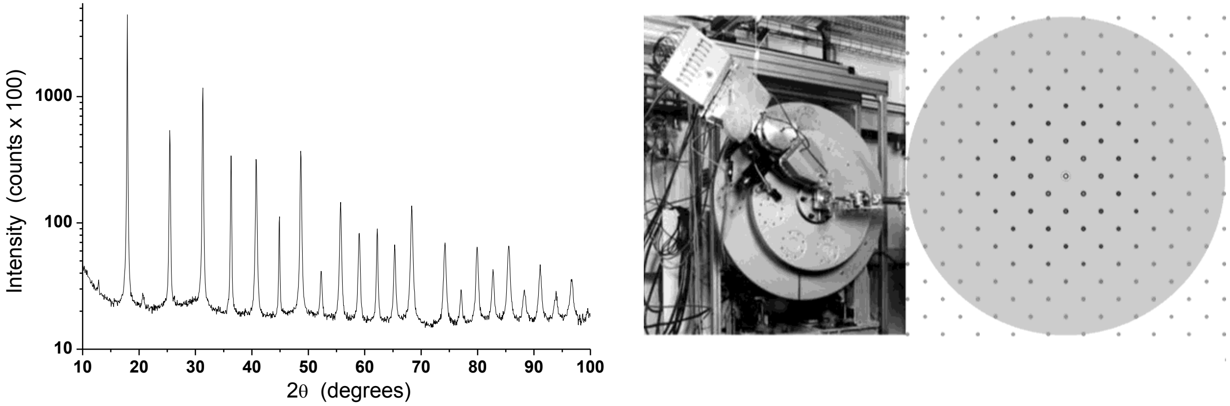

Powder diffraction data from a ball milled Fe1.5%Mo powder collected (b) on ID31 (now ID22) at ESRF, Grenoble (F) (λ=0.0632 nm). On the right: schematic of reciprocal space with extension of the limiting sphere (radius 2/λ).

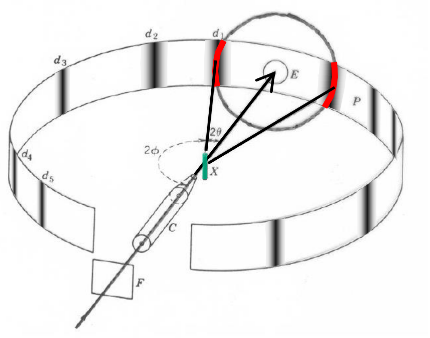

1916 Debye-Scherrer geometry
(the return !)

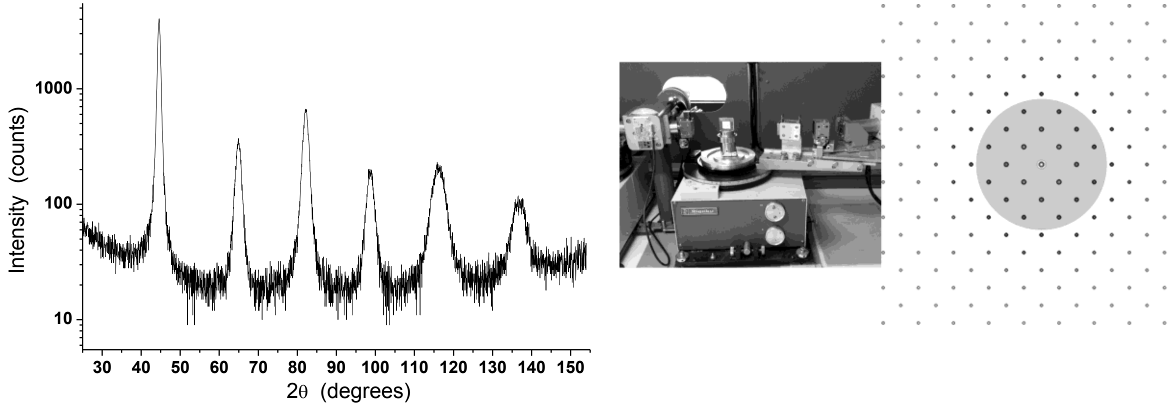

Powder diffraction data from a ball milled Fe1.5%Mo powder collected on a traditional laboratory instrument (Rigaku PMG-VH, Bragg-Brentano geometry) with CuKα radiation (λ=0.1540598 nm). On the right: schematic of reciprocal space with extension of the limiting sphere (radius 2/λ).

Fig. 1 in P. Scardi & L. Gelisio, Chapter XVIII, "Diffraction from nanocrystalline materials"

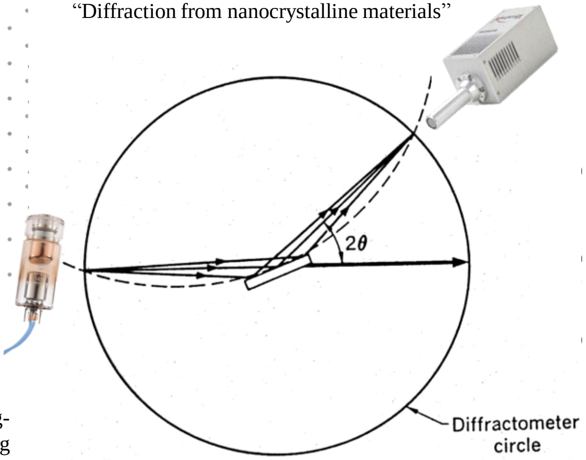

Powder diffractometer geometry

LABORATORY vs SYNCHROTRON RADIATION XRD

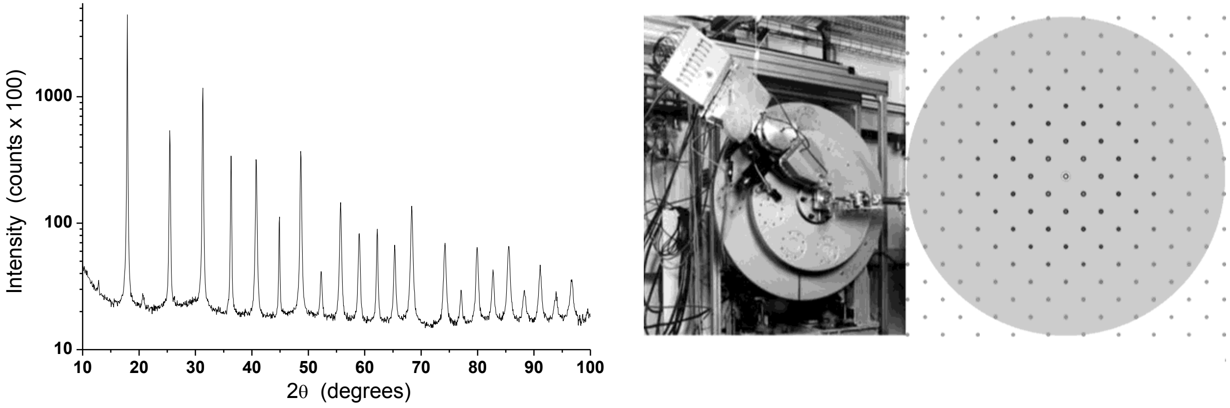

Powder diffraction data from a ball milled Fe1.5%Mo powder collected (b) on ID31 (now ID22) at ESRF, Grenoble (F) (λ=0.0632 nm).
On the right: schematic of reciprocal space with extension of the limiting sphere (radius $2/\lambda$).

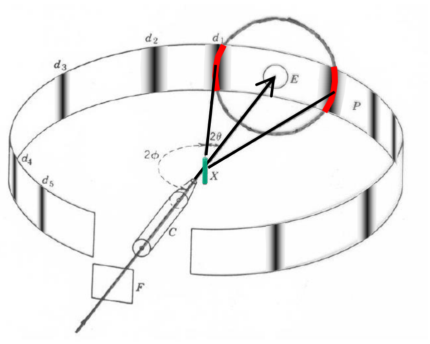

1916 Debye-Scherrer geometry
(the return !)

- **High intensity (brilliancy)**: better counting statistics / shorter data collection time (→ fast kinetics, in situ/in operando studies)
- **Highly collimated beam**: narrow instrumental profile for high resolution / accuracy (in the measurement of peak position, intensity, width, and shape)
- **High energy X-rays**: to extend the accessible region of reciprocal space (collect more peaks, more information, proper evaluation of asymptotic trend of intensity in PDF analysis, etc.)
- **Tuning X-ray energy**: e.g., for haldling absoprtion problems, or to exploit absorption thresholds (anomalous scattering)

DIFFRACTION FROM NANOCRYSTALLINE *POWDER*

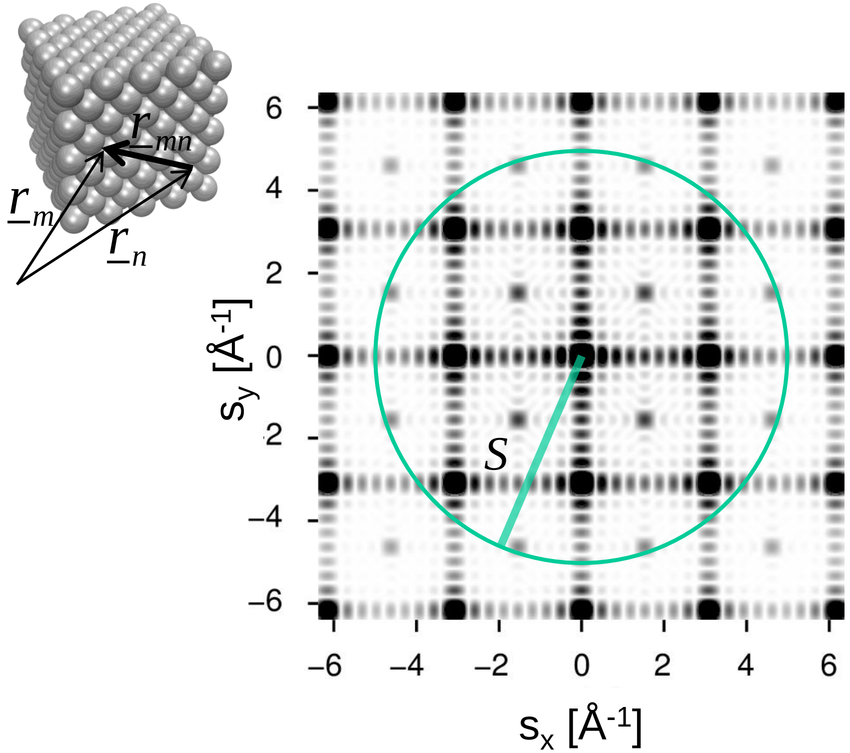

s=Q/2π=2sinθ /λ

$$I_{PD}(s) \propto \frac{\int \sum_m \sum_n f_m f_n^* e^{2\pi i(\underline{s}\cdot\underline{r}_{mn})} d\Omega}{4\pi s^2}$$

$$d\Omega = s^2 \sin\vartheta \, d\vartheta \, d\phi$$

$$I_{sc}(\underline{s}) \propto \sum_m f_m e^{2\pi i(\underline{s}\cdot\underline{r}_m)} \sum_n f_n^* e^{-2\pi i(\underline{s}\cdot\underline{r}_n)} = \sum_m \sum_n f_m f_n^* e^{2\pi i(\underline{s}\cdot\underline{r}_{mn})}$$

DIFFRACTION FROM NANOCRYSTALLINE *POWDER*

Traditional "reciprocal space" approach: factorize unit cell intensity

F, the structure factor

Intensity from one unit cell, $I_{uc} \propto |F|^2$

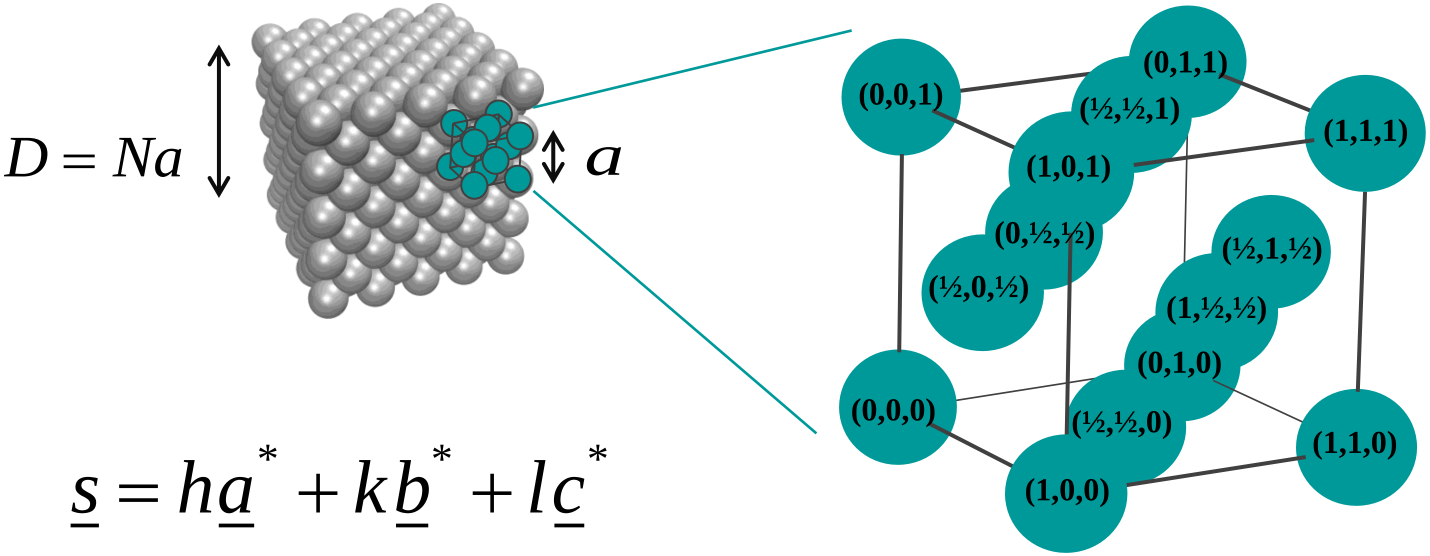

(u_n, v_n, w_n)

$$\underline{s} = h\underline{a}^* + k\underline{b}^* + l\underline{c}^*$$

$$\underline{r}_n = u_n\underline{a} + v_n\underline{b} + w_n\underline{c}$$

$$I_{uc}(\underline{s}) = \sum_m f_m e^{2\pi i(\underline{s}\cdot\underline{r}_m)} \sum_n f_n^* e^{-2\pi i(\underline{s}\cdot\underline{r}_n)} = \left|\sum_{n=1}^{N} f_n e^{2\pi i(u_n h + v_n k + w_n l)}\right|^2 = |F|^2$$

DIFFRACTION FROM NANOCRYSTALLINE *POWDER*

Factorize structural contribution: the line profile function

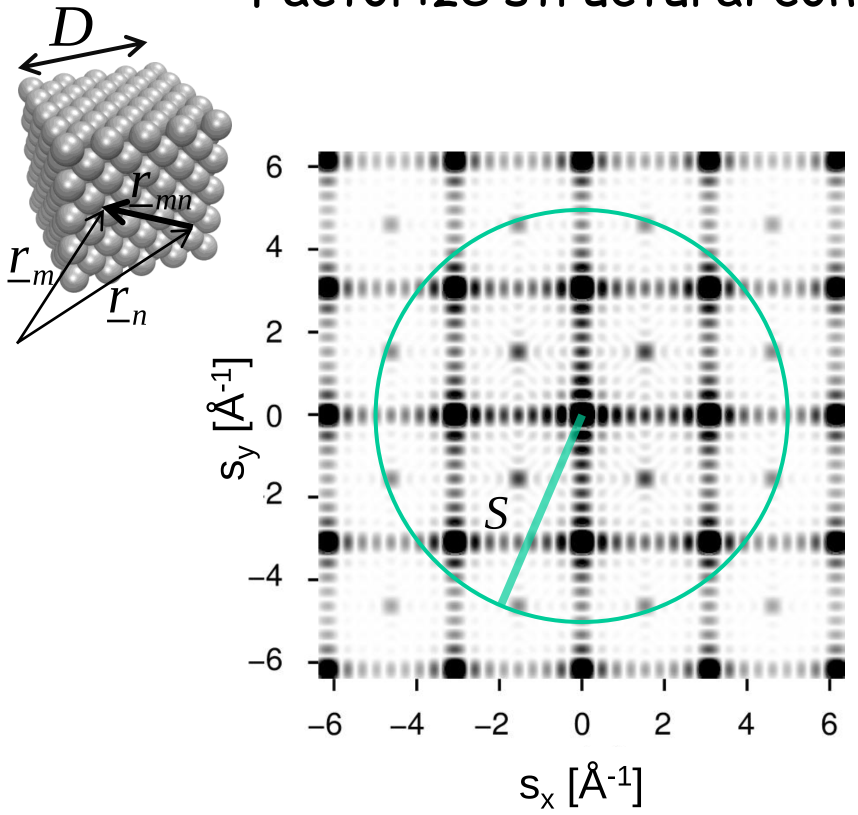

$$I_{PD}(s) \propto \frac{\int \sum_m \sum_n f_m f_n^* e^{2\pi i(\underline{s}\cdot\underline{r}_{mn})}\, d\Omega}{4\pi s^2}$$

$$\boxed{\approx |F|^2 \underbrace{\Phi(s,D)}_{\text{line profile function}}}$$

DIFFRACTION FROM NANOCRYSTALLINE *POWDER*

Fourier Transform of peak profile: the Common Volume Function

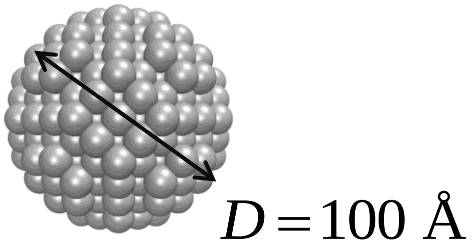

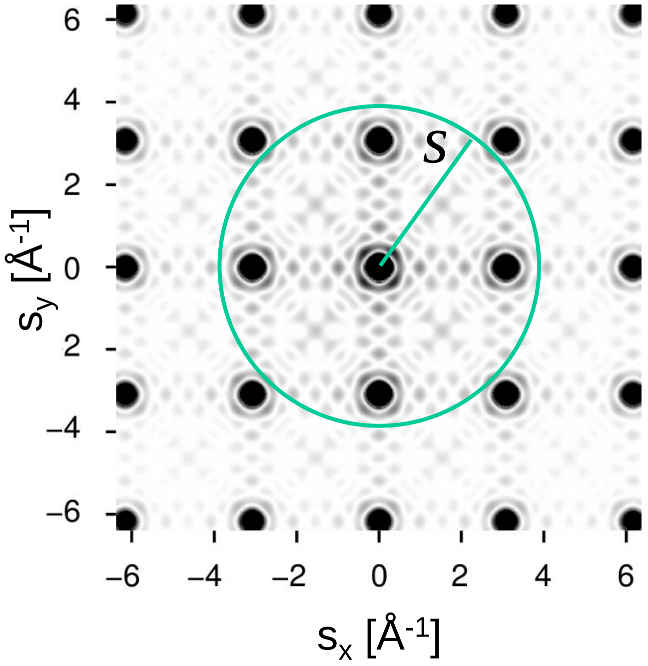

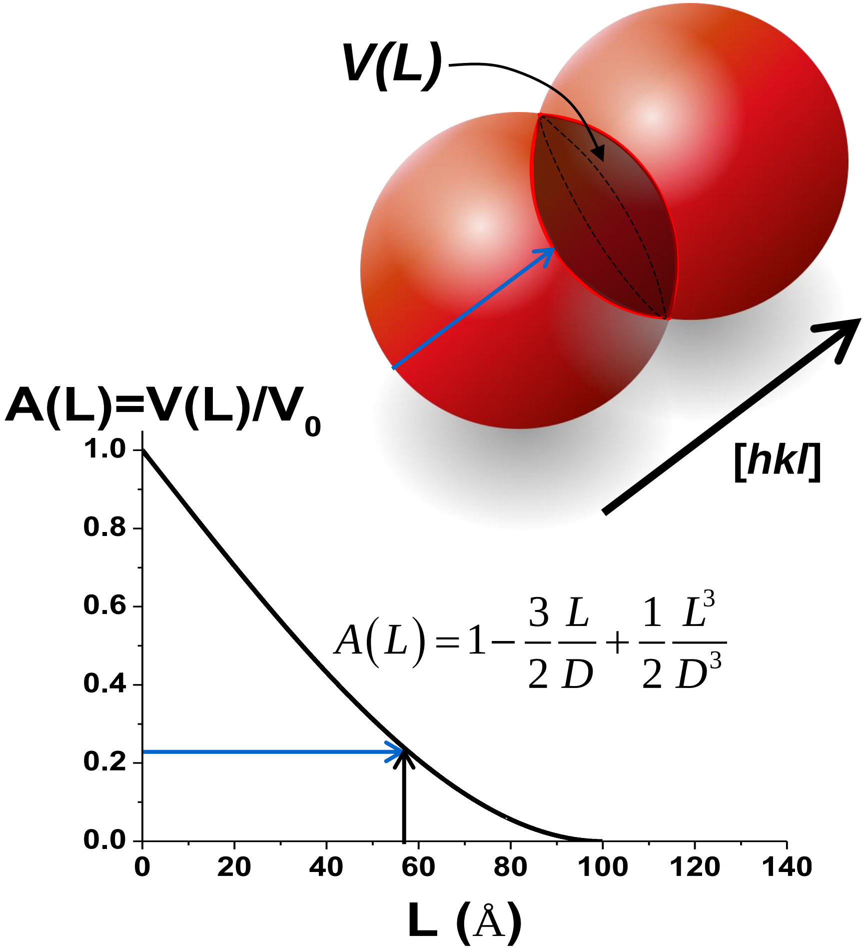

$$I_{PD}(s) \propto |F|^2\,\Phi_{sphere}(s,D) \quad = |F|^2 \int_0^D A(L)\cos(2\pi sL)\,dL$$

DIFFRACTION FROM NANOCRYSTALLINE *POWDER*

Fourier Transform of peak profile: the Common Volume Function

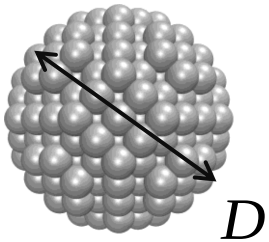

$$D = 100\ \text{Å}$$

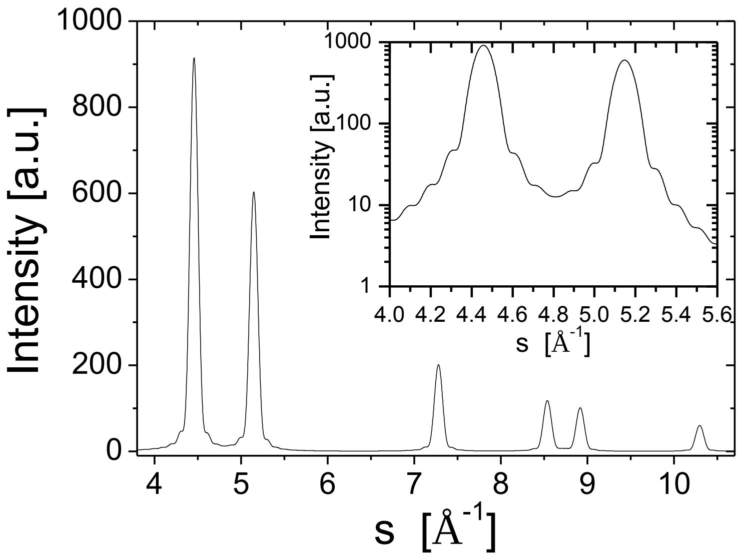

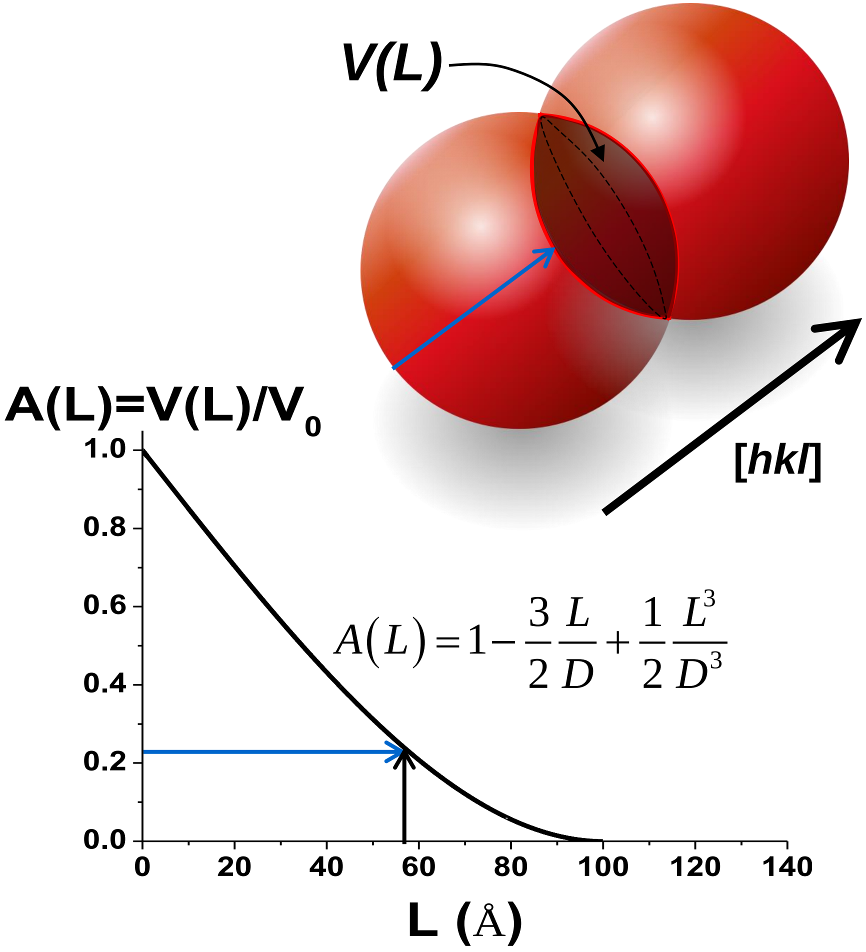

$$I_{PD}(s) \propto |F|^2 \Phi_{sphere}(s,D) \quad = |F|^2 \int_0^D A(L)\cos(2\pi sL)\,dL$$

DIFFRACTION FROM NANOCRYSTALLINE *POWDER*

ESRF - ID31 (now ID22)

λ=0.0632 nm

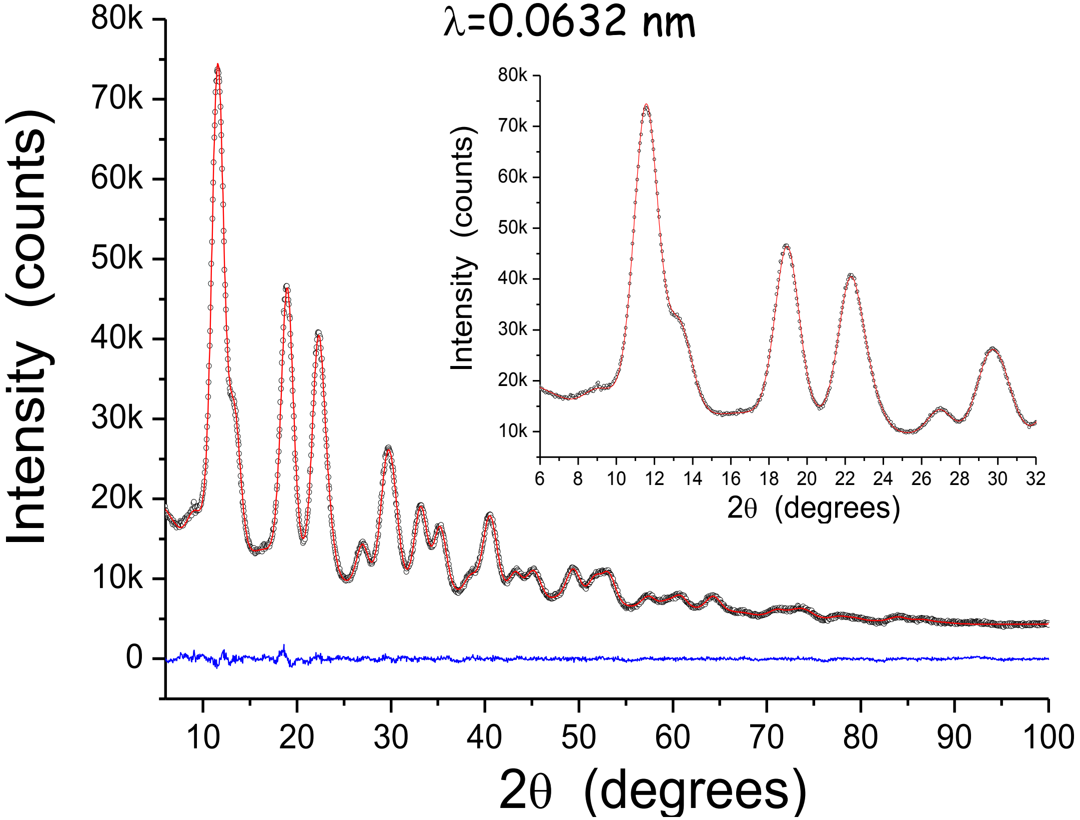

Xerogel cerium oxide powder

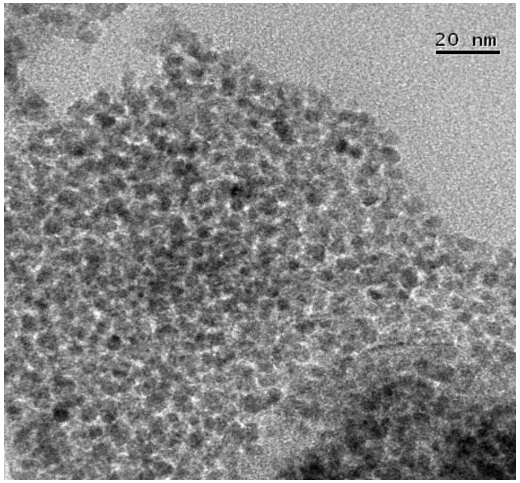

$$g(D)=\frac{1}{D\sigma(2\pi)^{1/2}}e^{-(\ln D-\mu)^2/2\sigma^2}$$

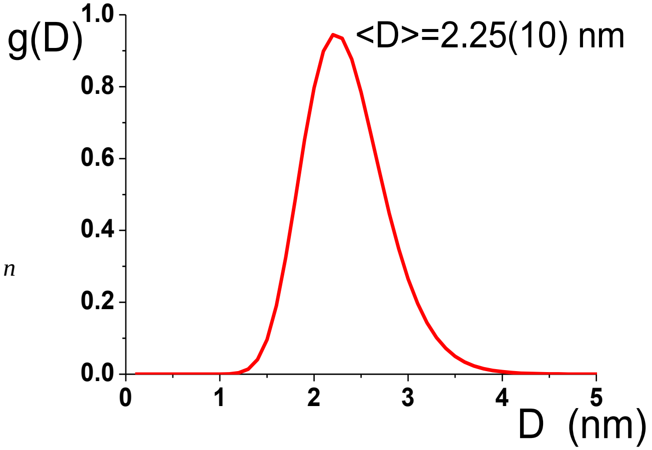

$$A_{ln,sphere}(L)=$$

$$\sum_{n=0}^{3}H_n\mathrm{erfc}\left[\frac{\ln|L|-\mu-(3-n)\sigma^2}{\sigma\sqrt{2}}\right]\exp\left\{-\frac{n}{2}\left[2\mu+(6-n)\sigma^2\right]\right\}|L|^n$$

$H_0=½, H_1=-¾, H_2=0, H_3=¼$

Scardi, P. (2008). Powder Diffraction: Theory and Practice, edited by R. E. Dinnebier & S. J. L. Billinge, ch. 13, pp. 376–413. Cambridge: Royal Society of Chemistry

DIFFRACTION FROM NANOCRYSTALLINE *POWDER*

Fourier Transform of peak profile: the Common Volume Function

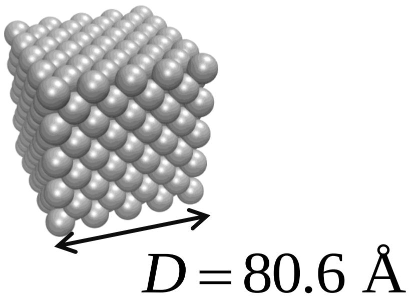

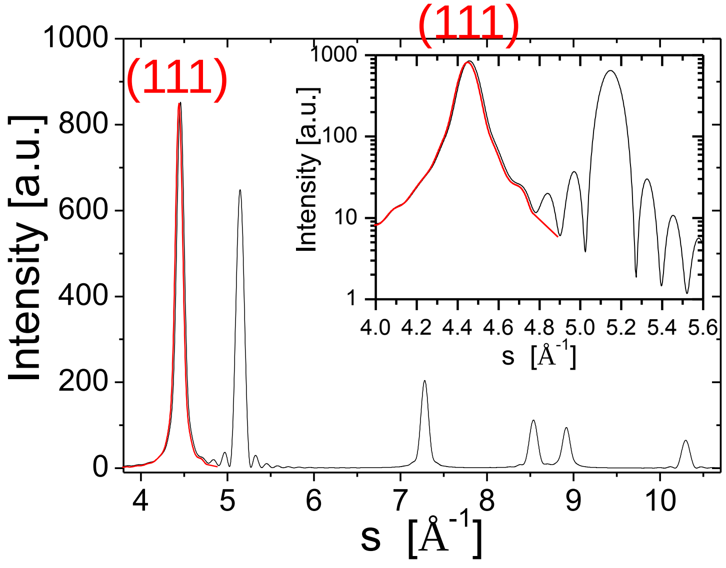

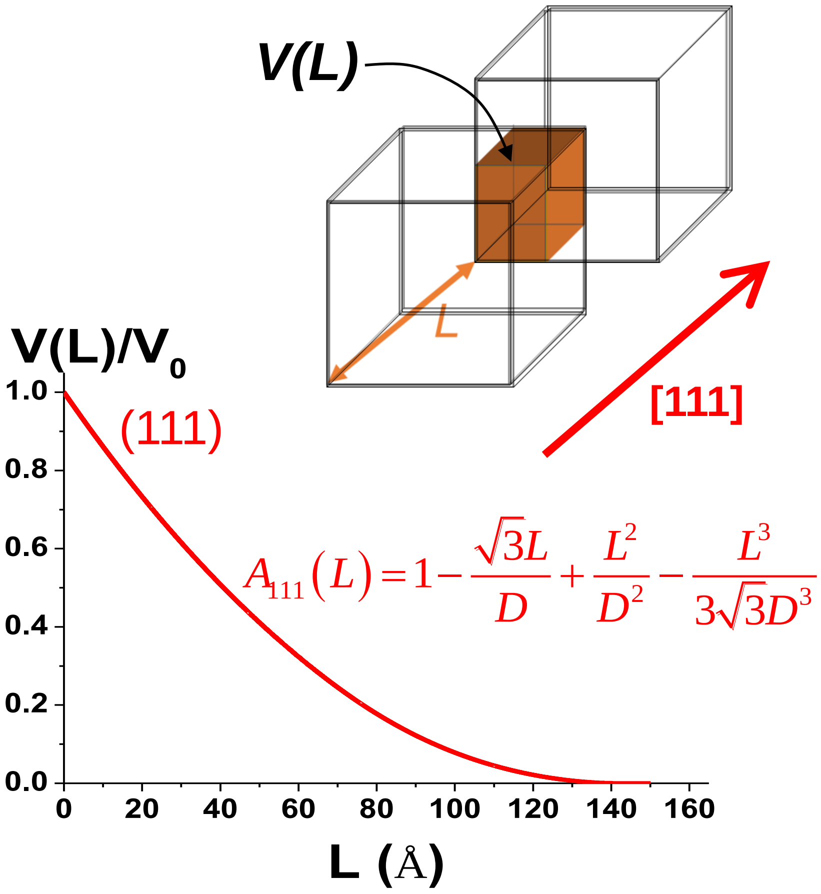

$$A_{111}(L) = 1 - \frac{\sqrt{3}L}{D} + \frac{L^2}{D^2} - \frac{L^3}{3\sqrt{3}D^3}$$

$$I_{PD}(s) \propto |F|^2 \Phi_{cube}(s,D) \quad = |F|^2 \int_0^{L_{\max}} A(L)\cos(2\pi s L)\, dL$$

DIFFRACTION FROM NANOCRYSTALLINE *POWDER*

Fourier Transform of peak profile: the Common Volume Function

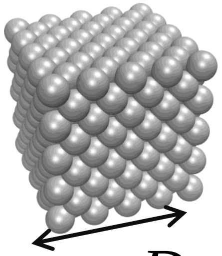

$D = 80.6\ \text{Å}$

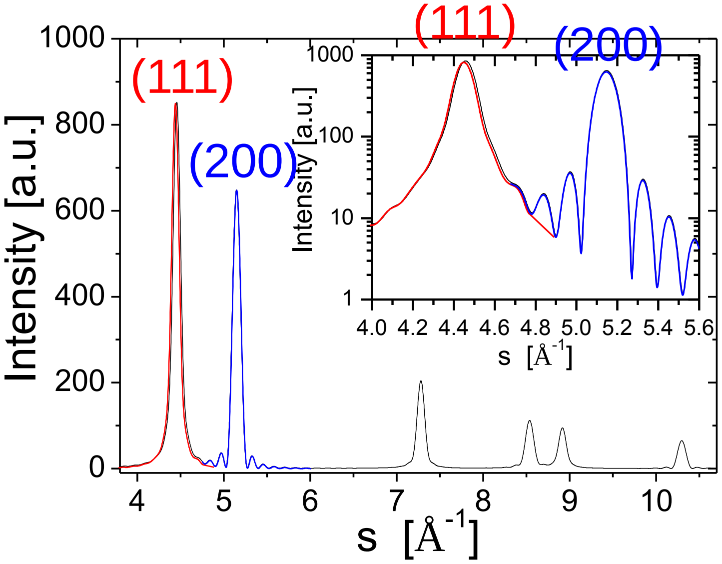

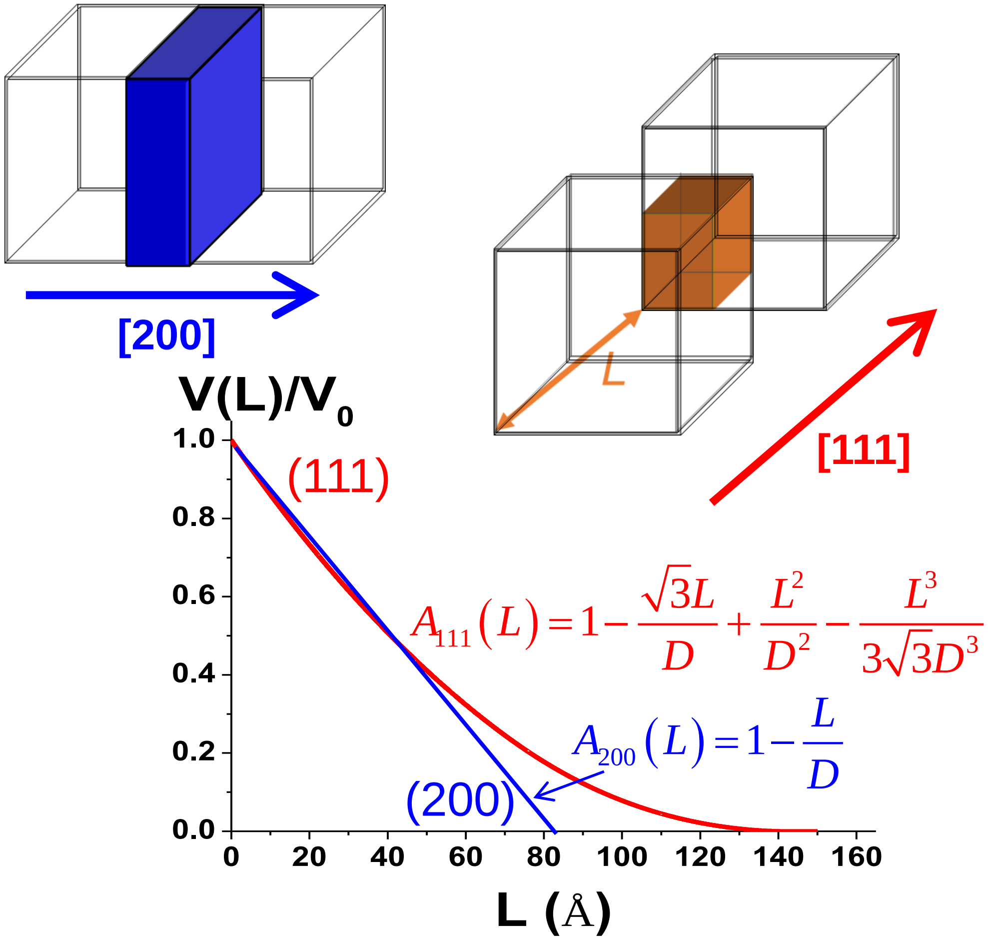

$$A_{111}(L) = 1 - \frac{\sqrt{3}L}{D} + \frac{L^2}{D^2} - \frac{L^3}{3\sqrt{3}D^3}$$

$$A_{200}(L) = 1 - \frac{L}{D}$$

$$I_{PD}(s) \propto |F|^2 \Phi_{cube}(s,D) \quad = |F|^2 \int_0^{L_{\max}} A(L)\cos(2\pi sL)\,dL$$

DIFFRACTION FROM NANOCRYSTALLINE *POWDER*

Any shape → A.Leonardi et al., J.Appl.Cryst. 45 (2012) 1162

Wulff polyhedra

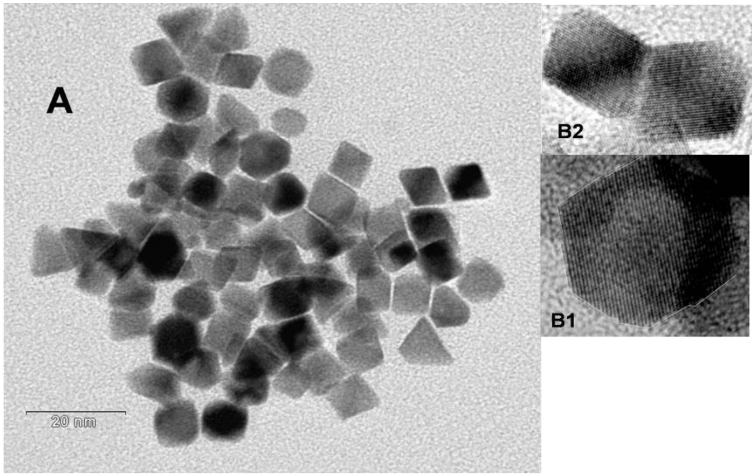

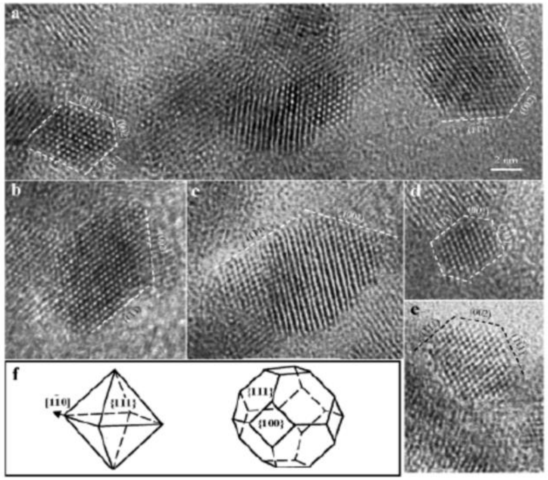

Figure 2. (a−e) Typical high-resolution TEM images of CeO_2 nanoparticles oriented along [110], showing the facet structures as defined by the {002} and {111} facets. (f) Structural models of the octahedral and truncated octahedral shapes.

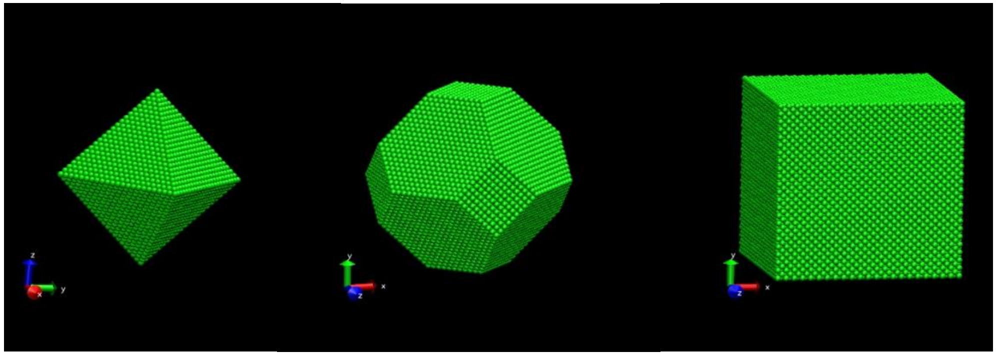

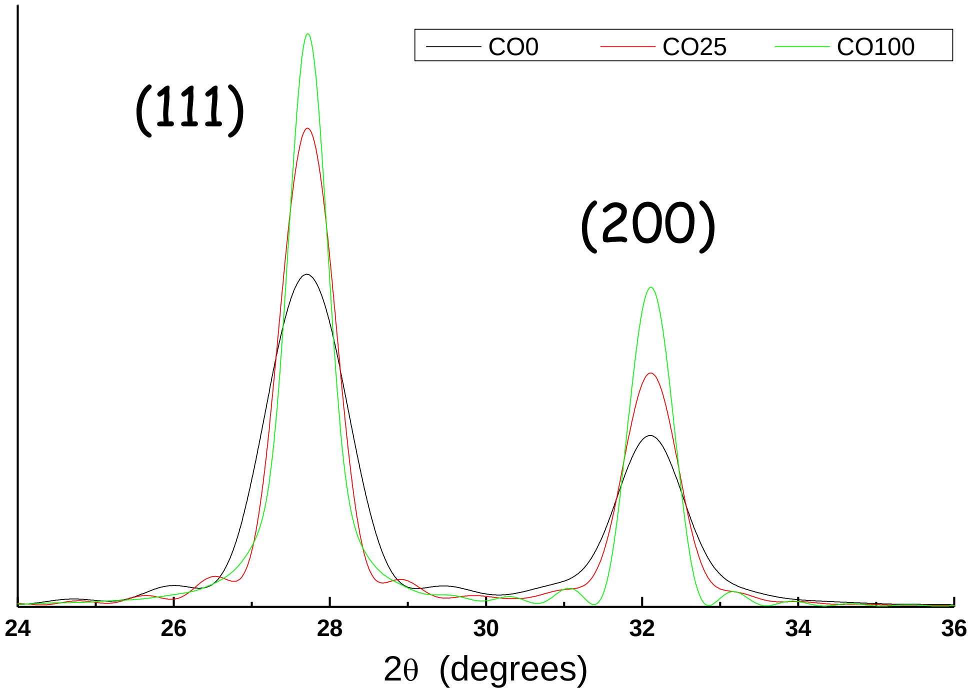

DIFFRACTION FROM NANOCRYSTALLINE *POWDER*

Pd nanocrystals

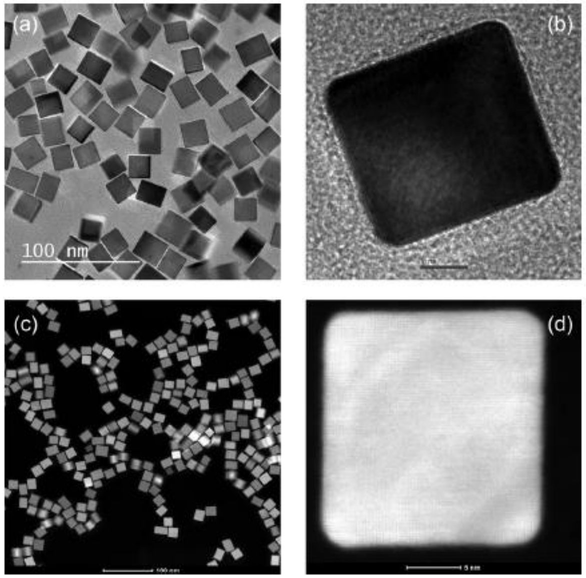

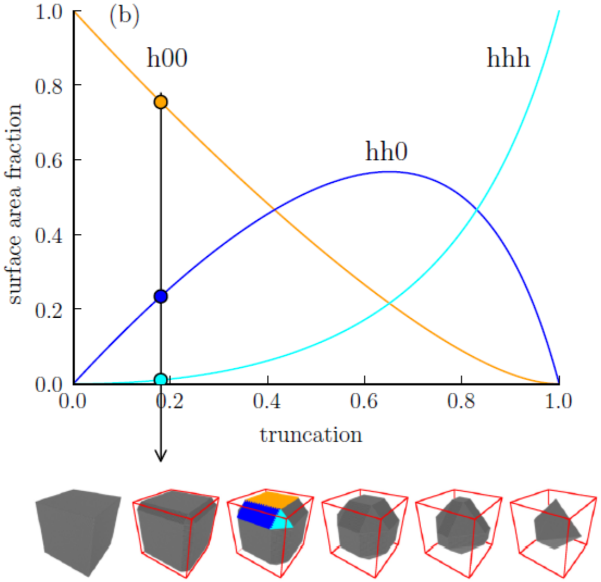

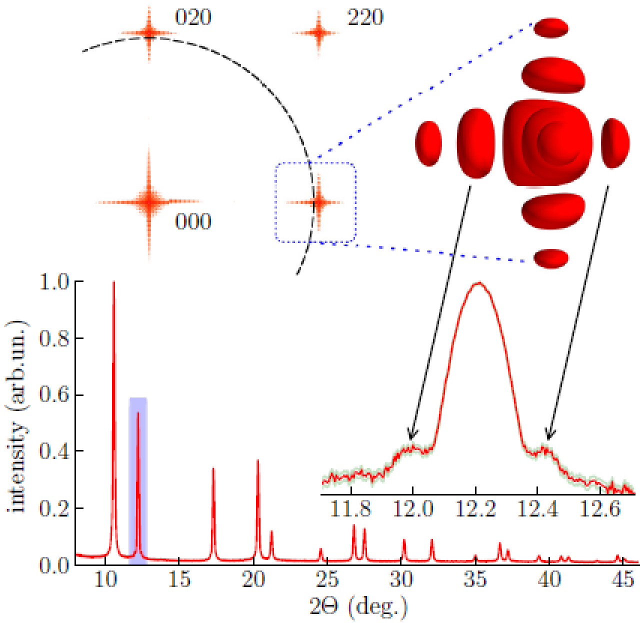

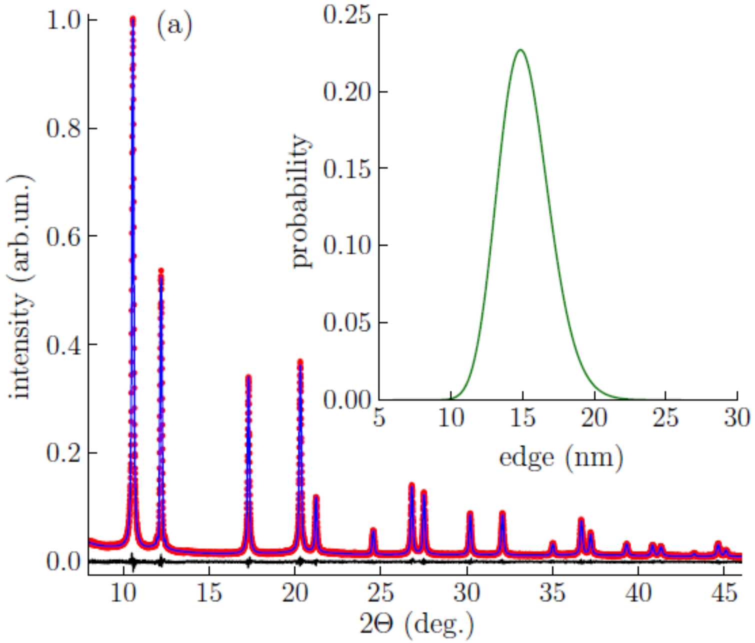

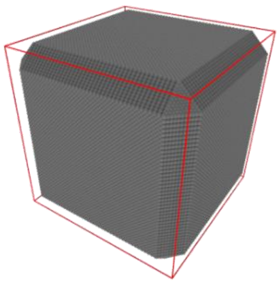

P. Scardi et al.
Phys.Rev.B 91(2015)155414

DIFFRACTION FROM NANOCRYSTALLINE *POWDER*

… what I did not consider (so far…): ***microstructure !***

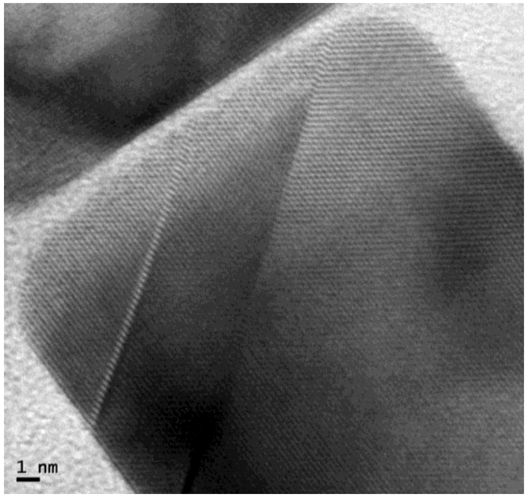

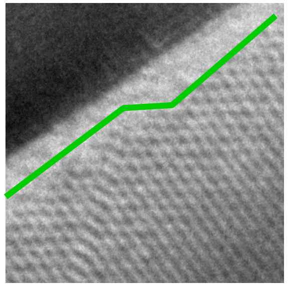

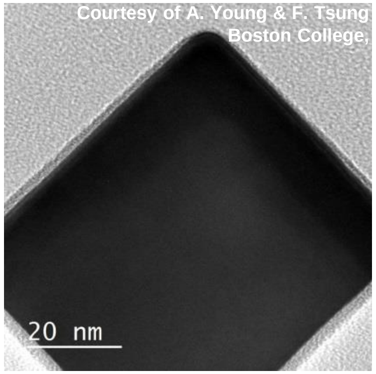
Courtesy of A. Young & F. Tsung Boston College,

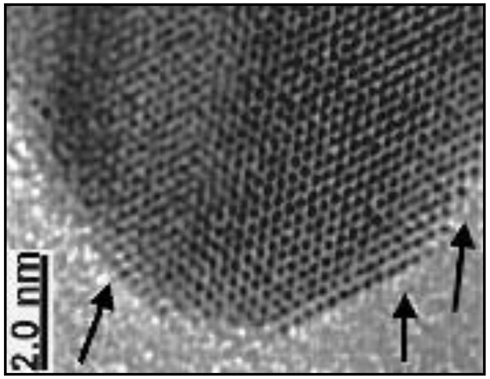

most metals:

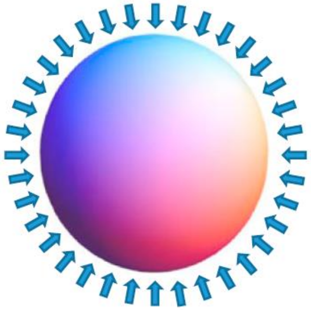

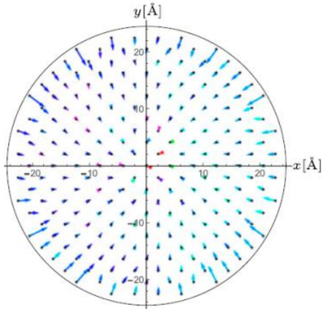

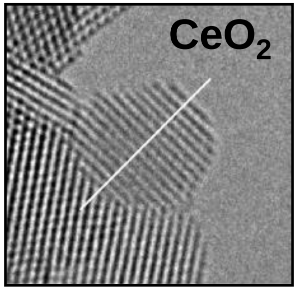

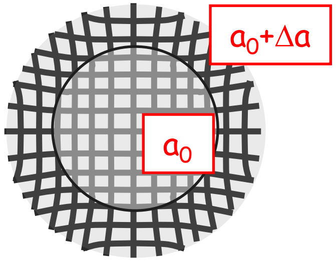

Surface relaxation
Perez-Demydenko & Scardi, Phil. Mag. 97 (2017) 2317

DIFFRACTION FROM NANOCRYSTALLINE *POWDER*

… what I did not consider (so far…): ***microstructure !***

Severe Plastic Deformation

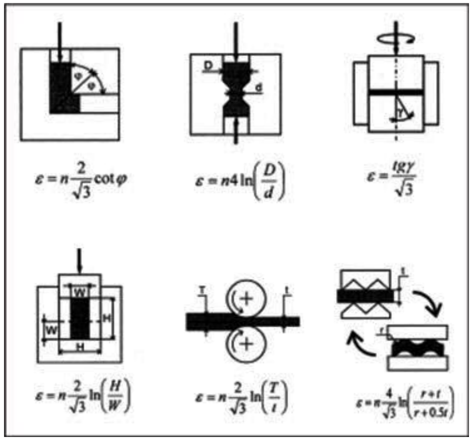

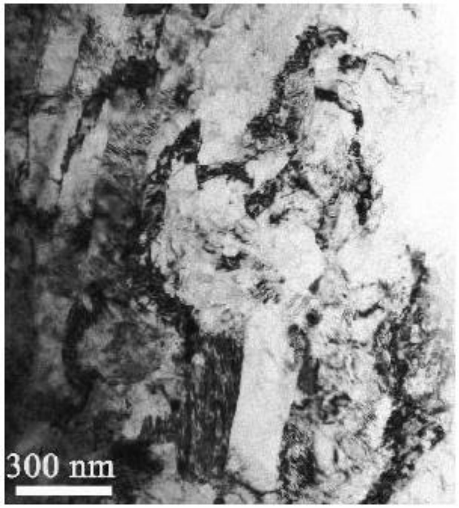

FIG. 1. Grain structures

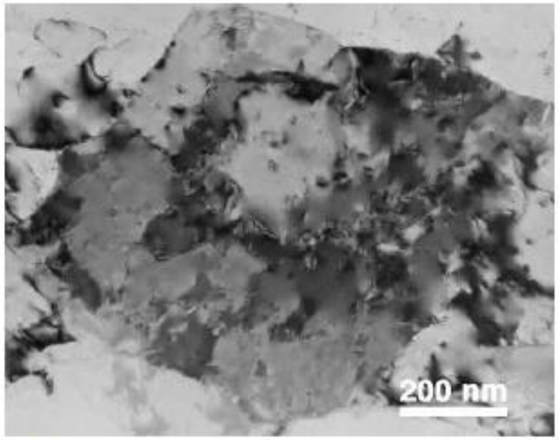

FIG. 8. Large grain containing several subgrains, which in turn contain dislocation cells.

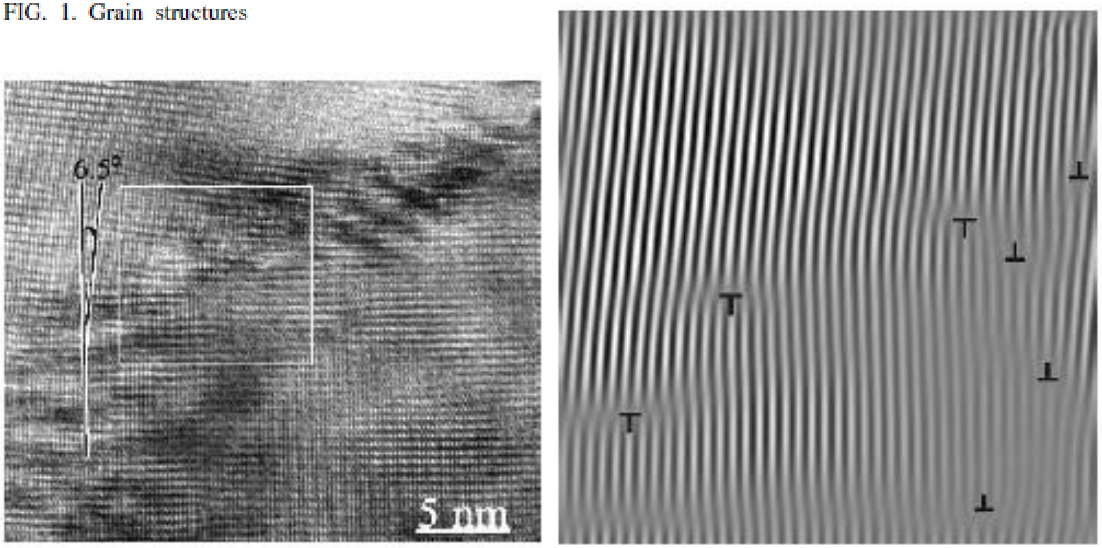

FIG. 10. (a) HRTEM image of a low-angle grain boundary with a misorientation of 6.5°, (b) Fourier-filtered image from the white frame in (a), showing the dislocation arrangement on the grain boundary

(Zhu et al. J. Mater. Res. 18 (2003) 1908)

DIFFRACTION FROM NANOCRYSTALLINE *POWDER*

microstructure → perturbation of “perfect crystal structure”

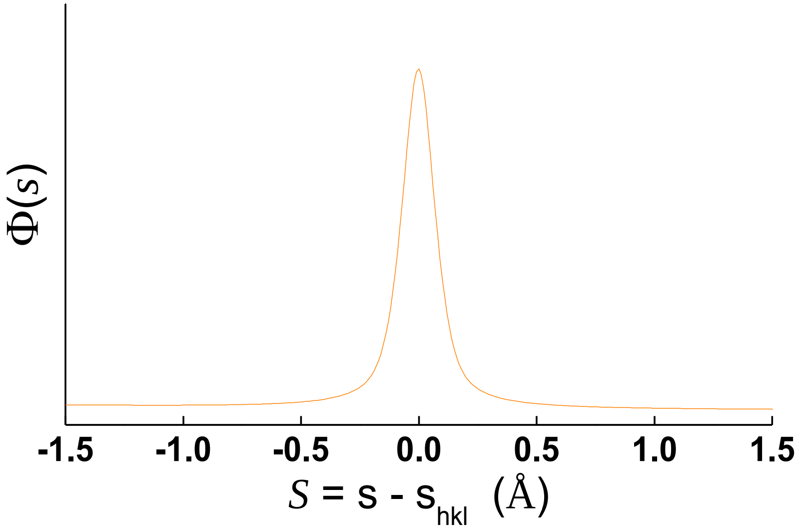

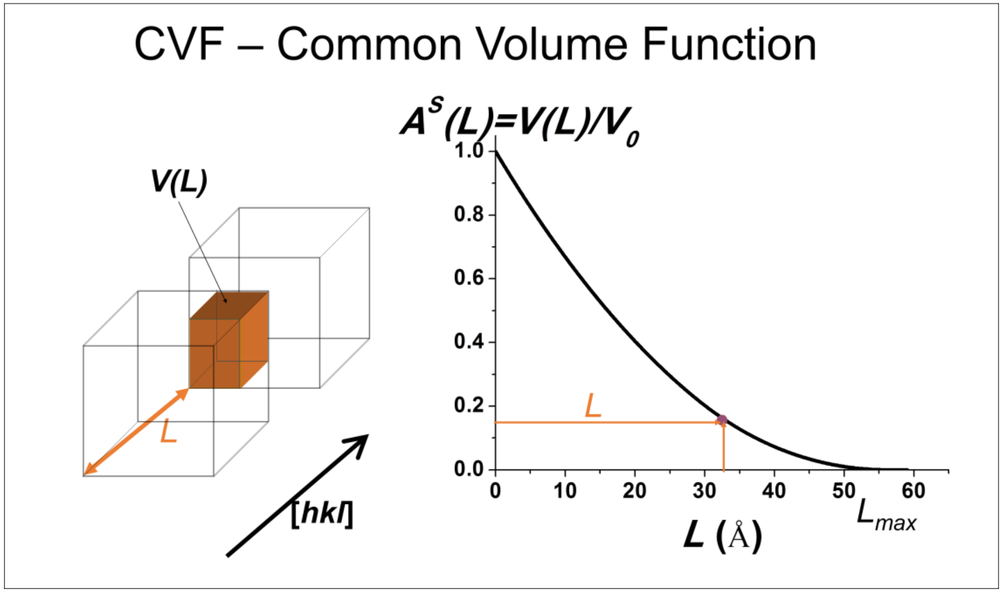

Any shape→ A.Leonardi et al., J.Appl.Cryst. 45 (2012) 1162

$$I(s)\propto|F|^2\int_0^{L_{\max}}A^S(L)\cos(2\pi sL)\,dL$$

⇓

$$I(s)\propto\int_0^{L_{\max}}A^S(L)\left\langle FF_L^*\right\rangle e^{2\pi isL}\,dL$$

$$I(s)\propto|F|^2\int_0^{L_{\max}}\underbrace{A^S}_{\text{domain size}}\overbrace{\left[\underbrace{A^D}_{\text{inhomog.strain}}\underbrace{(A^F+iB^F)}_{\text{faulting}}\cdot\ldots\right]}e^{2\pi isL}\,dL$$

DIFFRACTION FROM NANOCRYSTALLINE *POWDER*

Pd nanocrystals

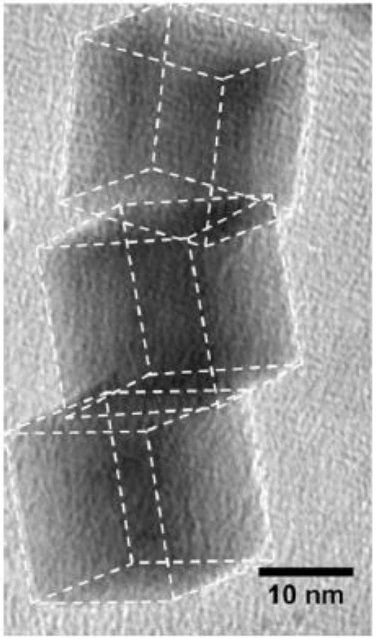

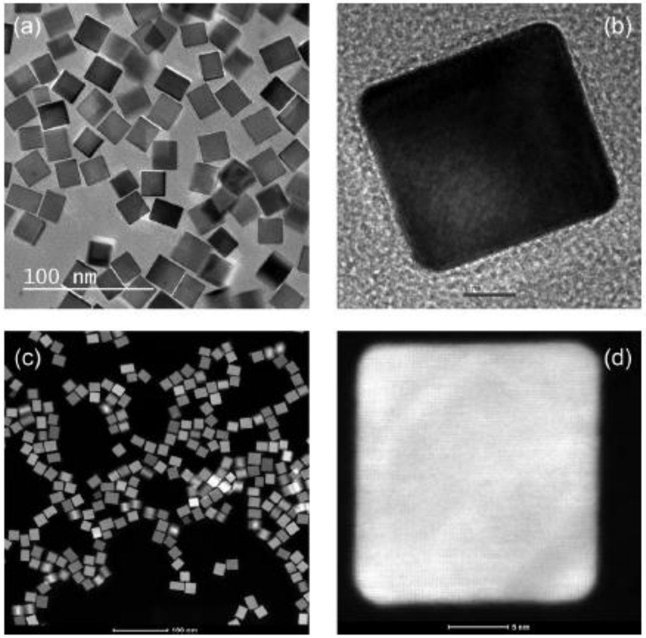

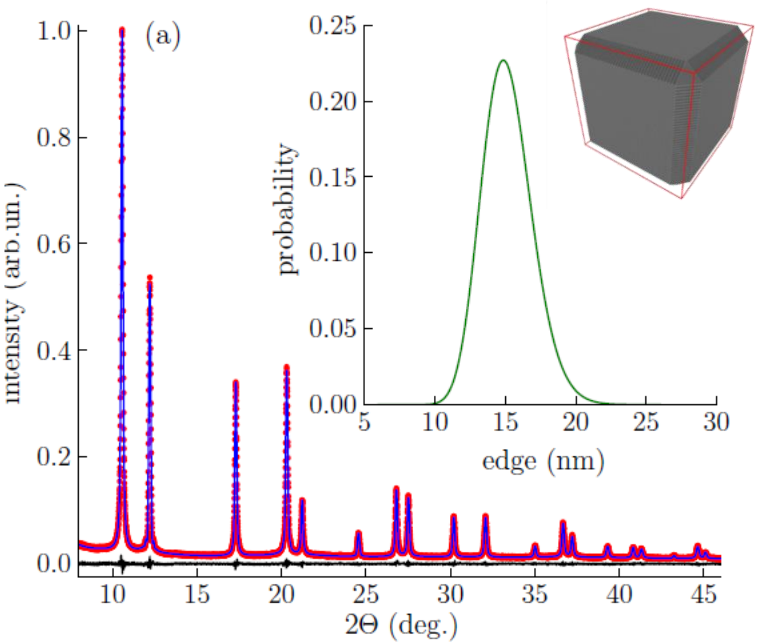

Inhomogeneous displacement
(strain, ε = ΔL/L): $A^D(L) = e^{-2\pi^2 s^2 <\Delta L_{hkl}^2>}$

$$I(s) \propto |F|^2 \int_0^{L_{\max}} \underbrace{A^S}_{\text{domain size}} \underbrace{A^D}_{\text{inhomog. strain}} \underbrace{T^{IP}}_{\text{instrum. profile}} e^{2\pi i s L} dL$$

P. Scardi et al. Phys.Rev.B 91(2015)155414

DIFFRACTION FROM NANOCRYSTALLINE *POWDER*

Pd nanocrystals

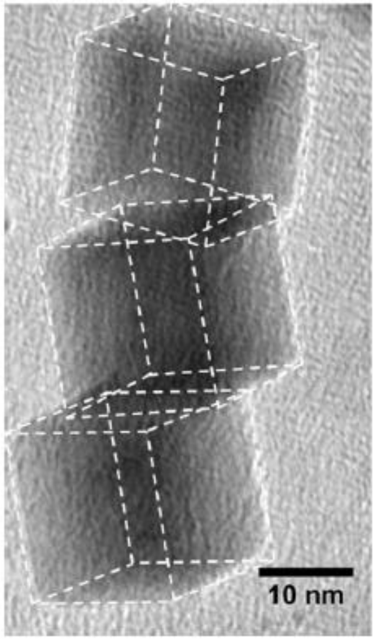

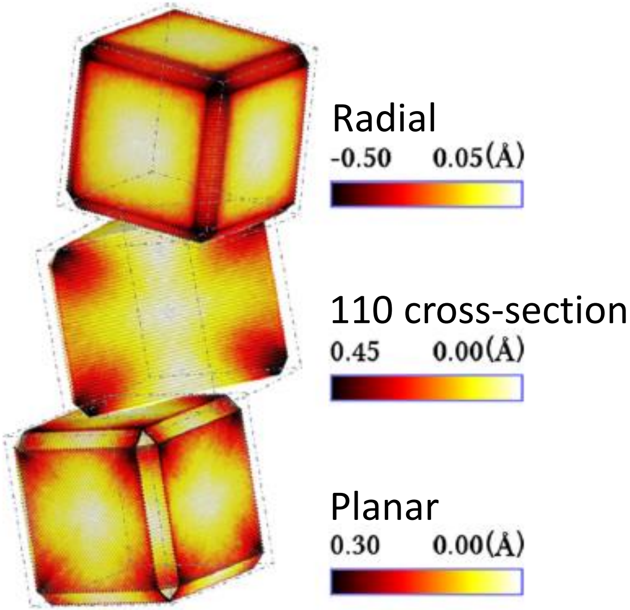

Molecular Dynamics (MD) atomic displacement maps

Warren plot

(root mean square displacement vs L)

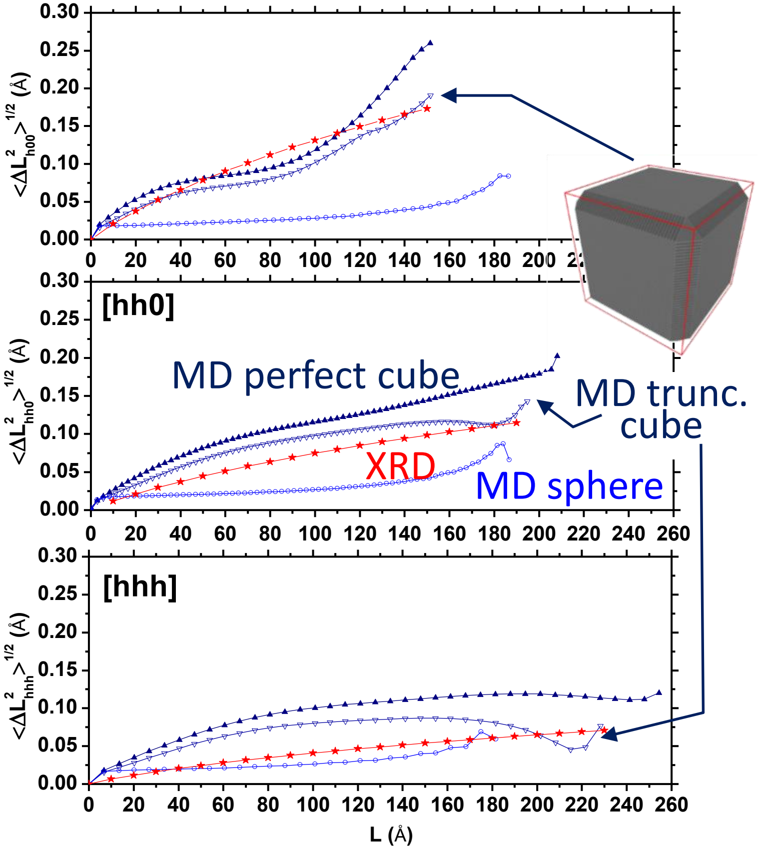

Inhomogeneous displacement
(strain, ε = ΔL/L): $A^D(L) = e^{-2\pi^2 s^2 <\Delta L^2_{hkl}>}$

$$I(s) \propto |F|^2 \int_0^{L_{\max}} A^S A^D T^{IP} e^{2\pi i s L} dL$$

domain size — inhomog. strain — instrum. profile

P. Scardi et al. Phys.Rev.B 91(2015)155414

WHOLE POWDER PATTERN MODELLING – WPPM

$$I(s) \propto |F|^2 \int_0^{L_{\max}} \underbrace{A^S}_{\text{domain size}} \Big[\underbrace{A^D}_{\text{inhomog.strain}} \underbrace{(A^F + iB^F)}_{\text{faulting}} \cdot \ldots \Big] \underbrace{T^{IP}}_{\text{instrum. profile}} e^{2\pi i s L} \, dL$$

Diffraction profile as a convolution of (independent) effects:

$$I(s) = I^{IP}(s) \otimes I^S(s) \otimes I^D(s) \otimes I^F(s) \otimes I^{APB}(s) \otimes \ldots$$

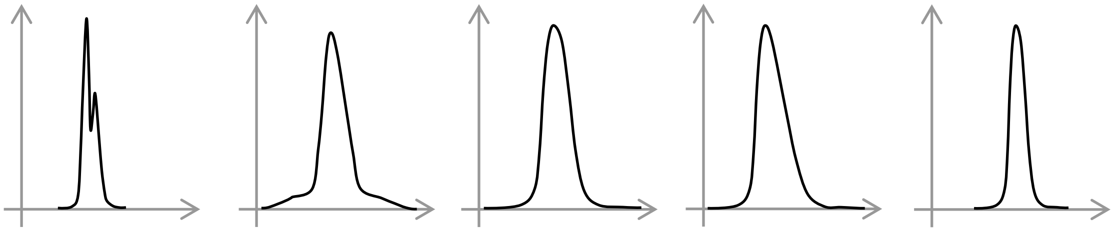

DIFFRACTION FROM NANOCRYSTALLINE *POWDER*

High-energy grinding (ball-milling) of an iron alloy powder: AstaloyTM Fe1.5Mo

SEM

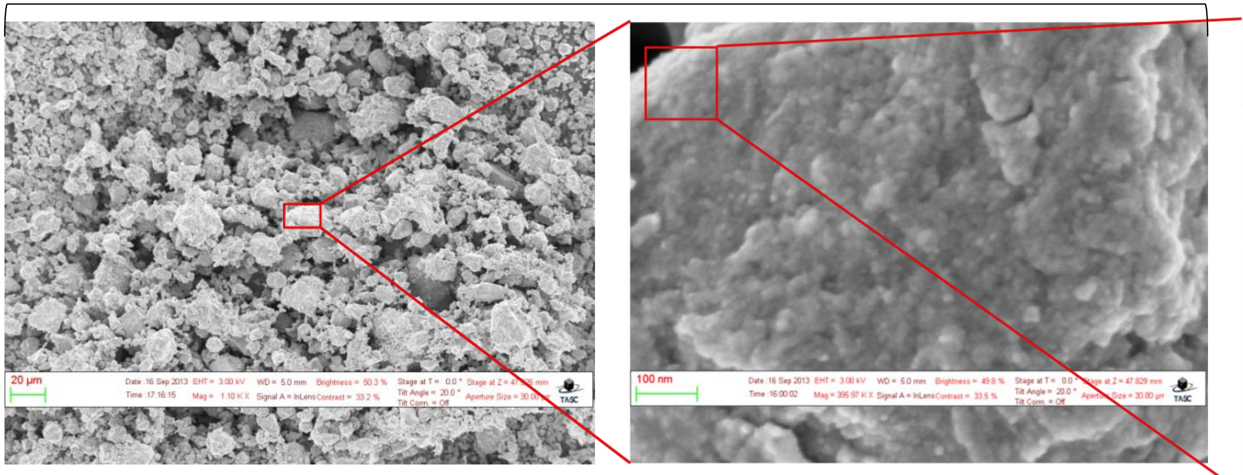

TEM

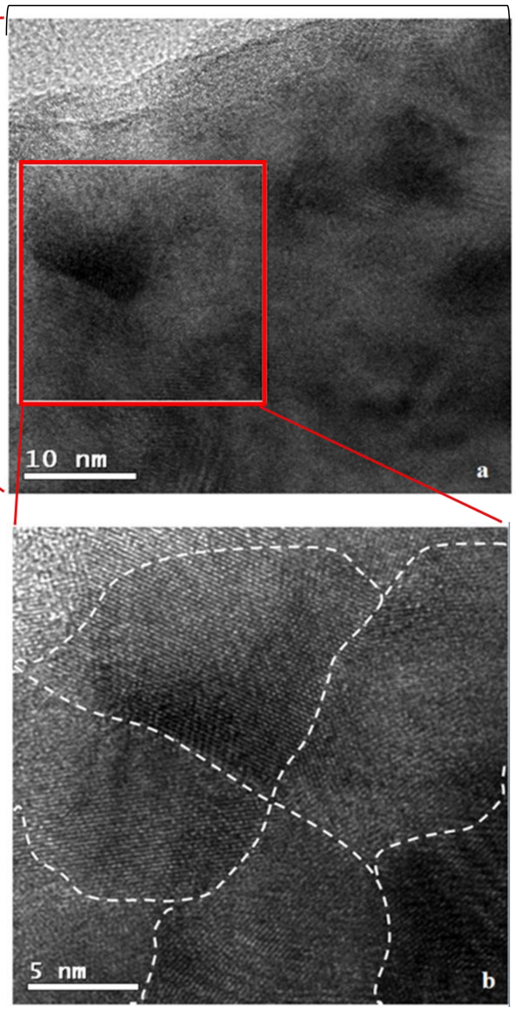

HREM

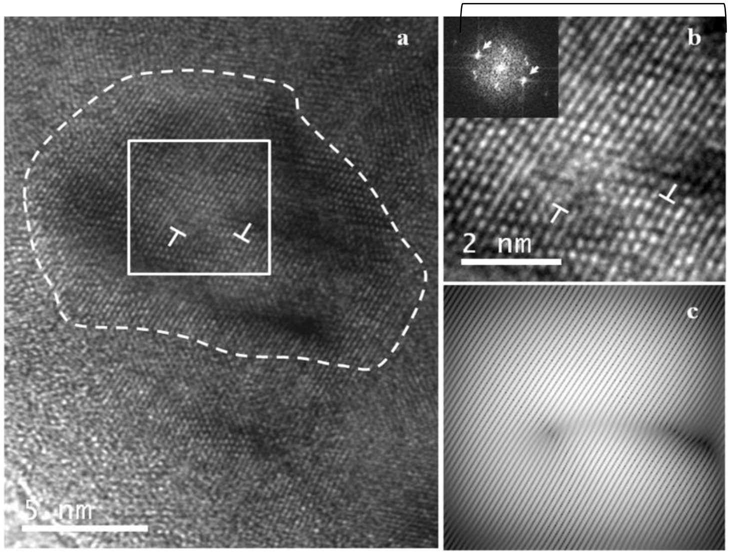

Rebuffi et al., Sci. Reports 6 (2016) 20712

DIFFRACTION FROM NANOCRYSTALLINE *POWDER*

High-energy grinding (ball-milling) of an iron alloy powder: AstaloyTM Fe1.5Mo

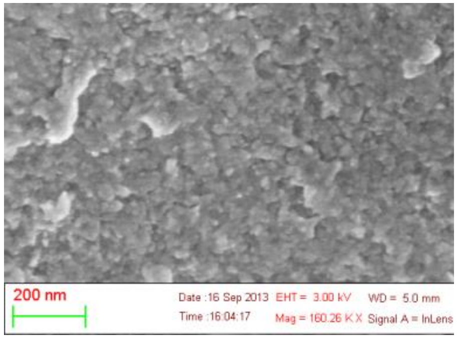

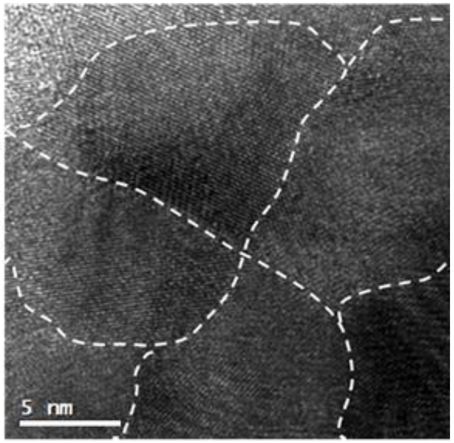

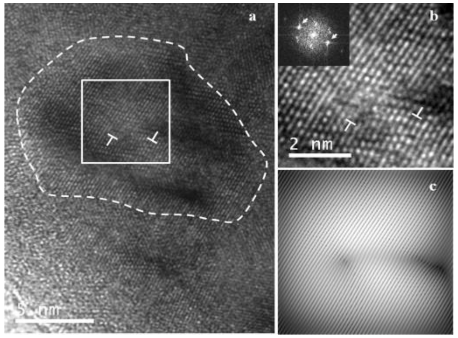

$$I_{hkl}(s) \propto |F|^2 \int A^S(L) A^D_{hkl}(L) T^{IP}(L) e^{2\pi isL} dL$$

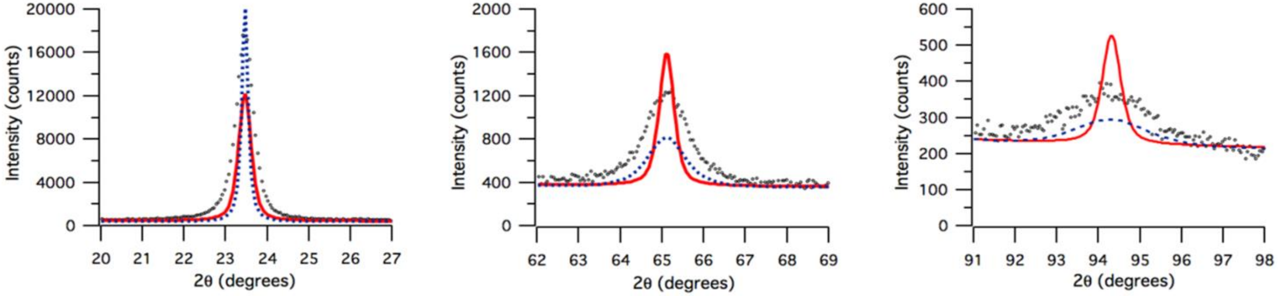

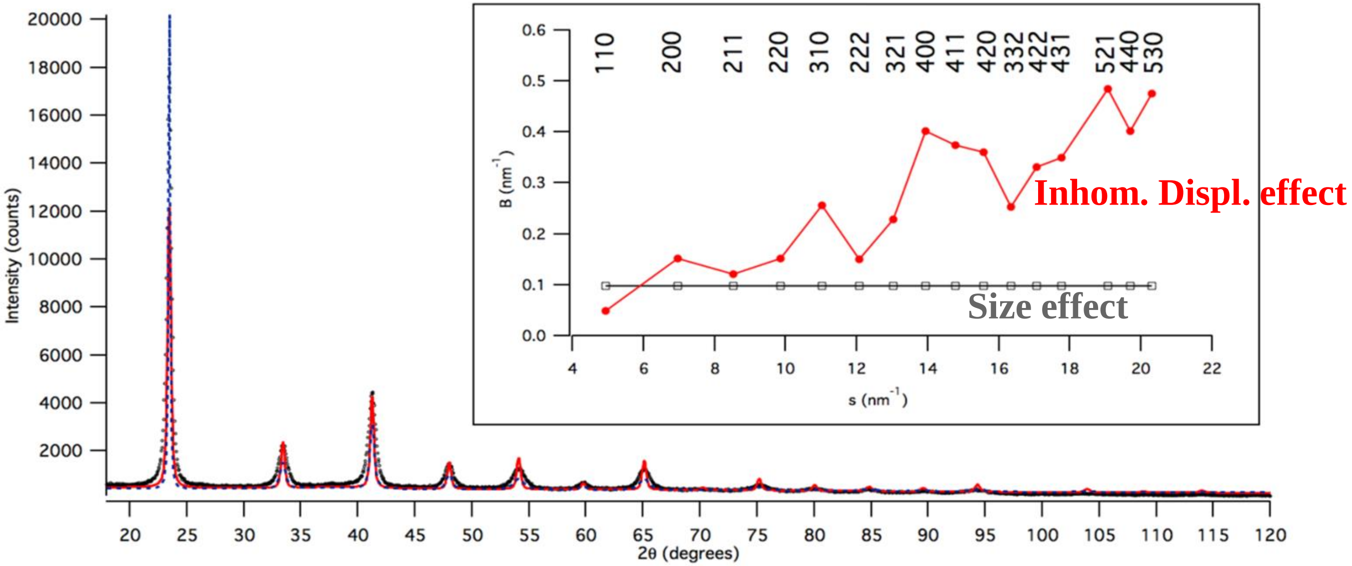

XRD data : MCX beamline, Italian synchrotron ELETTRA

Rebuffi et al., Sci. Reports 6 (2016) 20712

DIFFRACTION FROM NANOCRYSTALLINE *POWDER*

High-energy grinding (ball-milling) of an iron alloy powder: AstaloyTM Fe1.5Mo

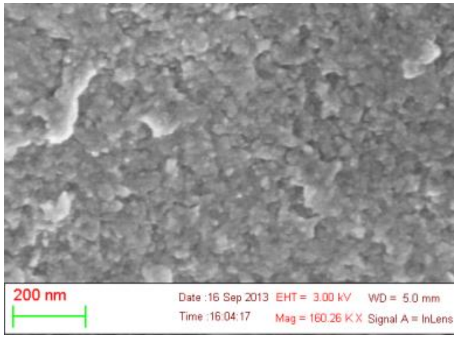

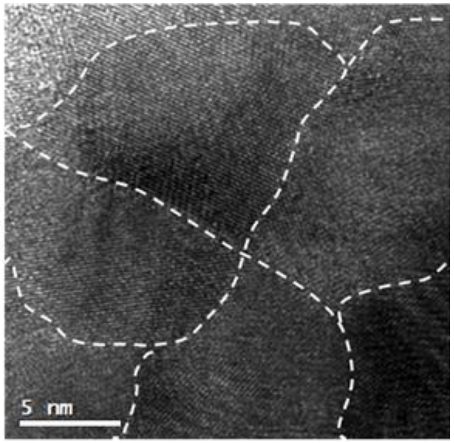

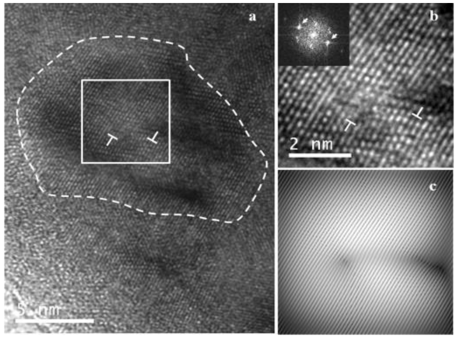

$$< \Delta L_{hkl}^{\ 2} > = \frac{\rho \overline{C}_{\{hkl\}} b^2}{4\pi} L^2 f^*\left(L/R_e\right)$$

ρ – average dislocation density

$\overline{C}_{\{hkl\}}$ – average contrast factor

b – Burgers vector modulus

R_e – effective outer cut-off radius

f^* – Wilkens' function

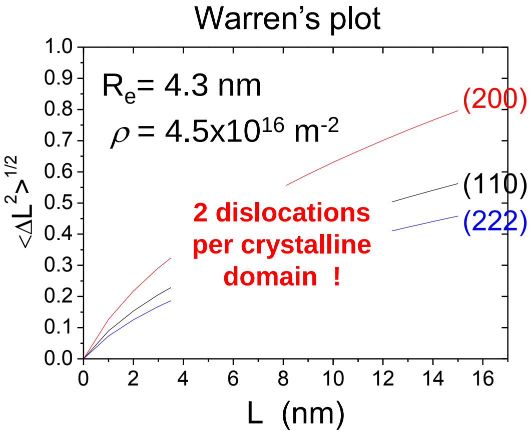

2 dislocations per crystalline domain !

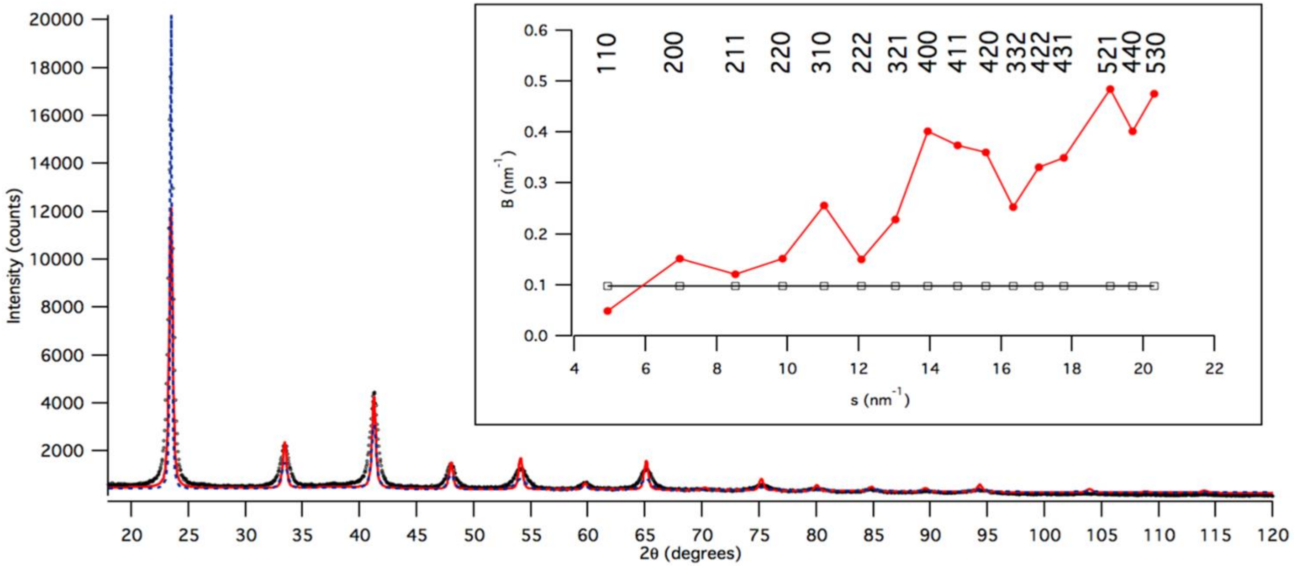

XRD data : MCX beamline, Italian synchrotron ELETTRA

Rebuffi et al., Sci. Reports 6 (2016) 20712

DIFFRACTION FROM NANOCRYSTALLINE *POWDER*

Understanding XRD line profile analysis result by Molecular Dynamics simulations

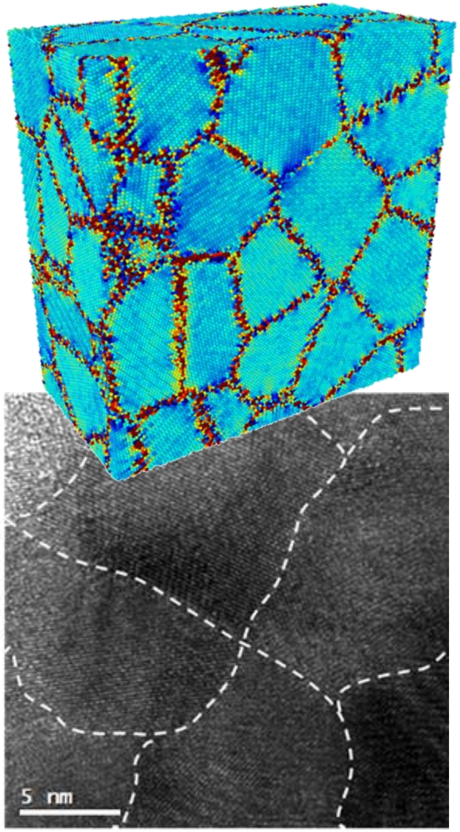

Molecular Dynamics (MD) simulation

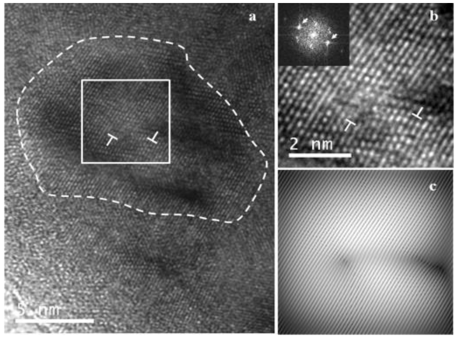

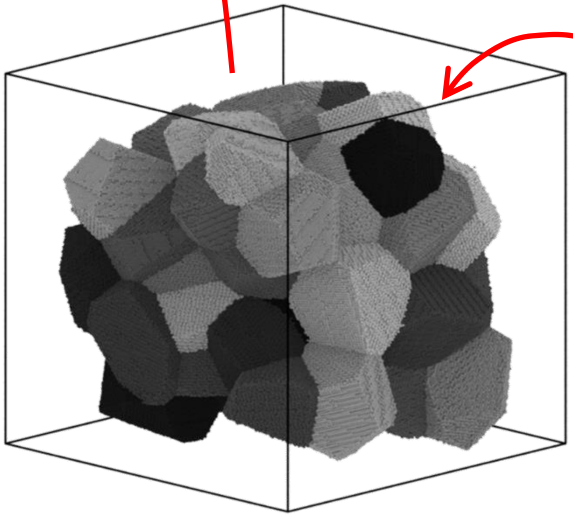

atomistic model
by space tessellation

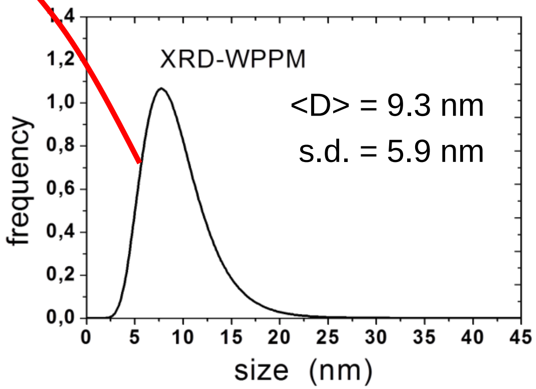

ICTP School - Trieste, 10.05.2018

Rebuffi et al., Sci. Reports 6 (2016) 20712

DIFFRACTION FROM NANOCRYSTALLINE ***POWDER***

Understanding XRD line profile analysis result by Molecular Dynamics simulations

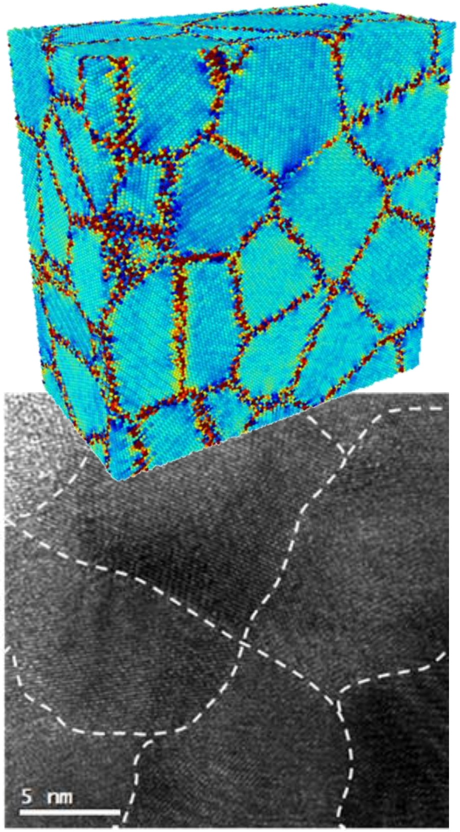

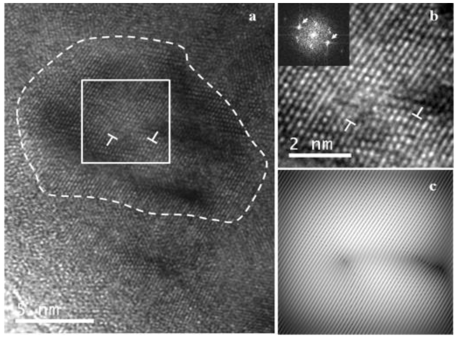

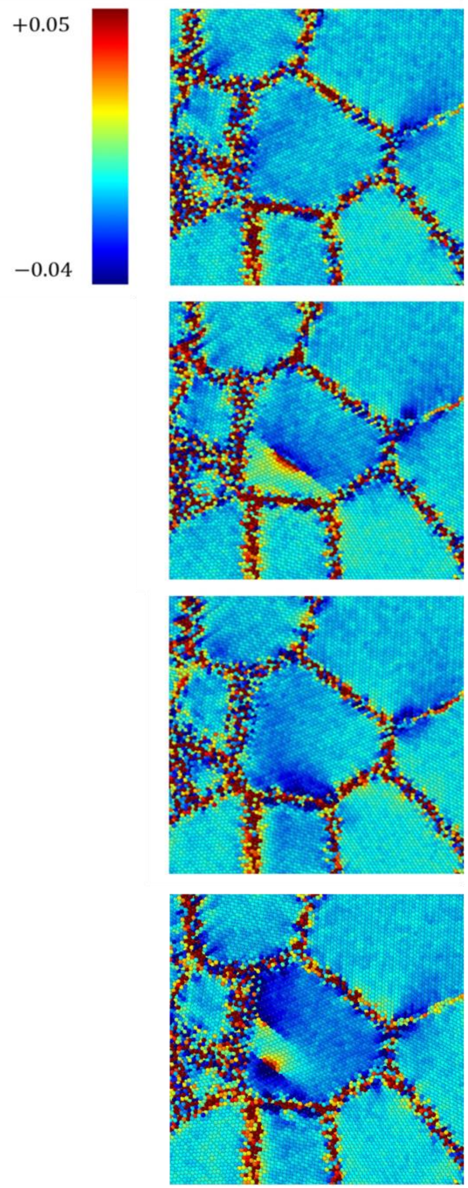

grain-grain interaction only

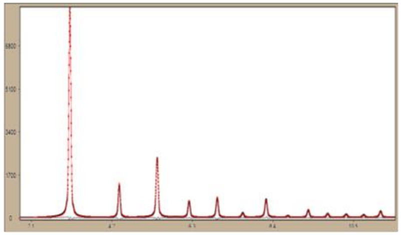

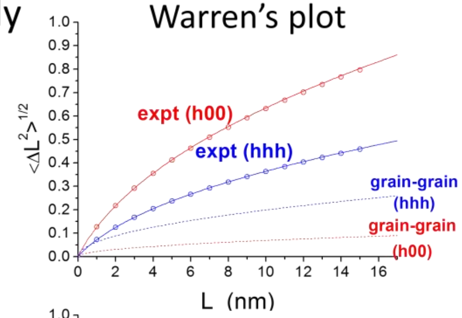
Warren's plot

1 edge dislocation

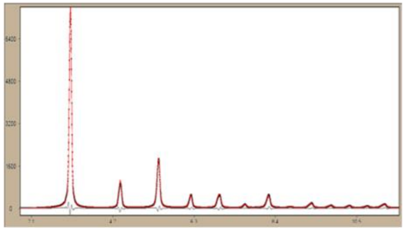

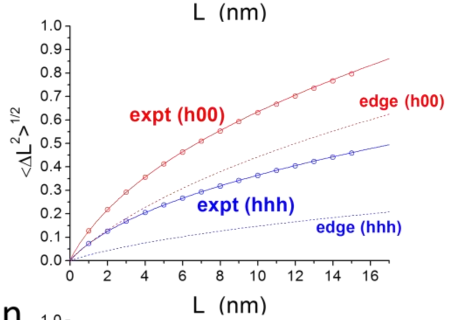

1 unstable edge dislocation

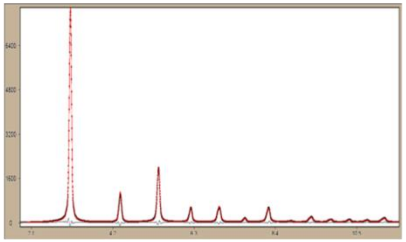

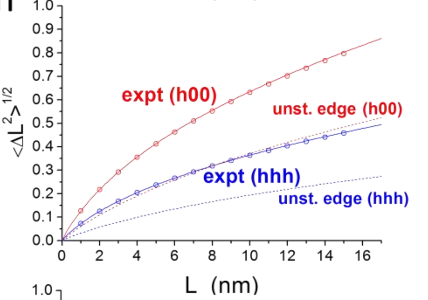

1 edge dislocation dipole

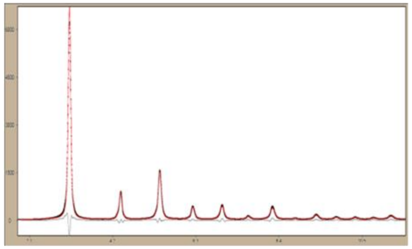

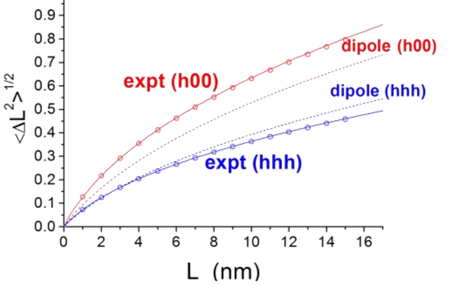

Rebuffi et al., Sci. Reports 6 (2016) 20712

DIFFRACTION FROM NANOCRYSTALLINE *POWDER*

Temperature Diffuse Scattering – TDS

Perfect Static Lattice

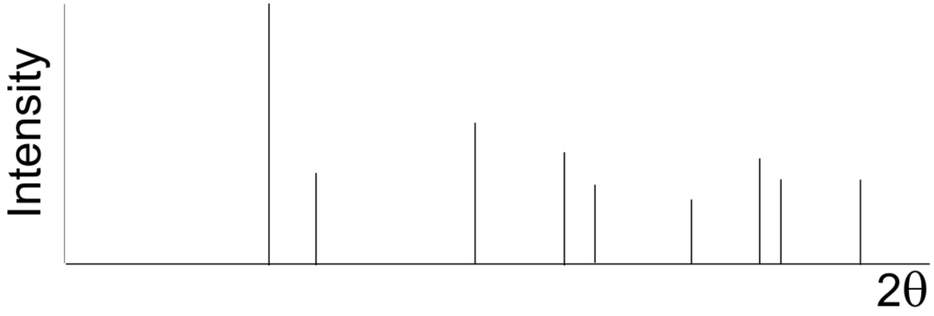

Random Atomic Motion

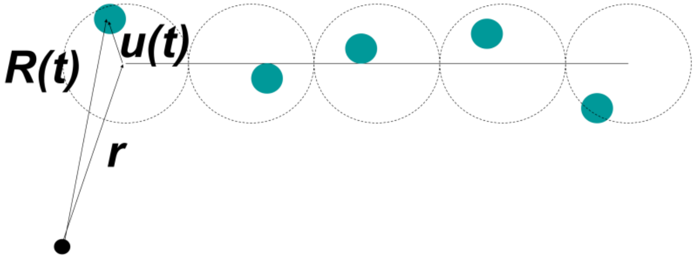

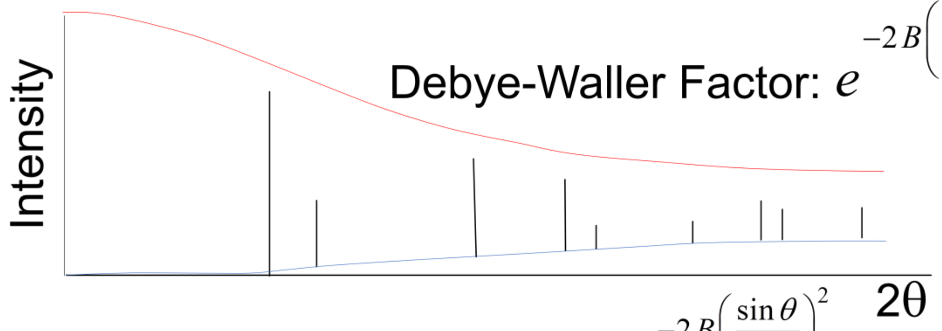

Debye-Waller Factor: $e^{-2B\left(\frac{\sin\theta}{\lambda}\right)^2}$

Debye TDS: $1-e^{-2B\left(\frac{\sin\theta}{\lambda}\right)^2}$

Correlated Atomic Motion

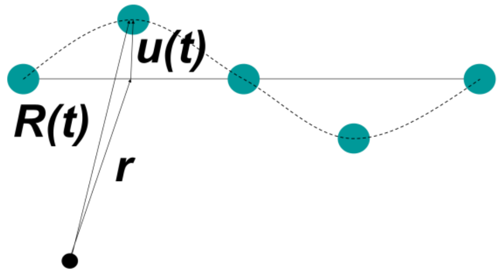

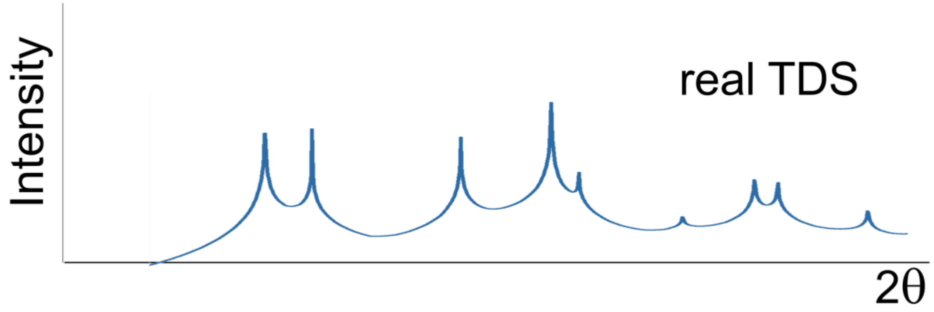

DIFFRACTION FROM NANOCRYSTALLINE *POWDER*

Temperature Diffuse Scattering – TDS in small crystals

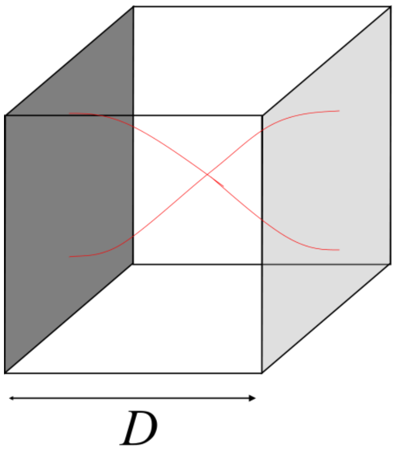

$$\lambda_{\max} \approx 2D$$

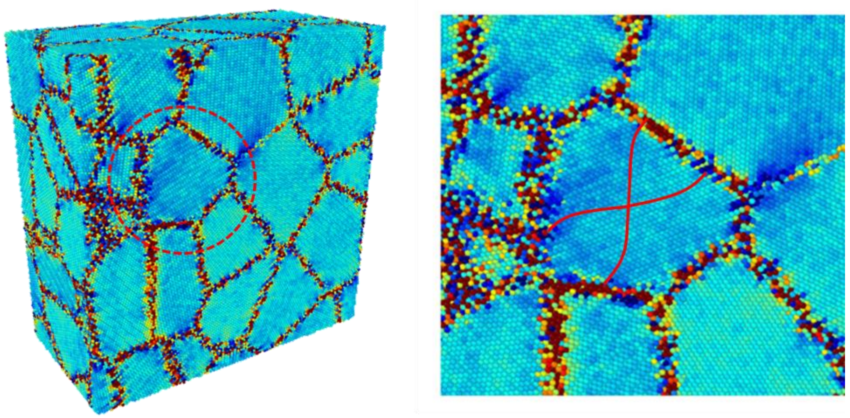

$$\omega_{\min} = 2\pi c_s(\omega)/\lambda_{\max} = \omega_{\min}(D)$$

small λ_{max} → truncation of TDS peaks

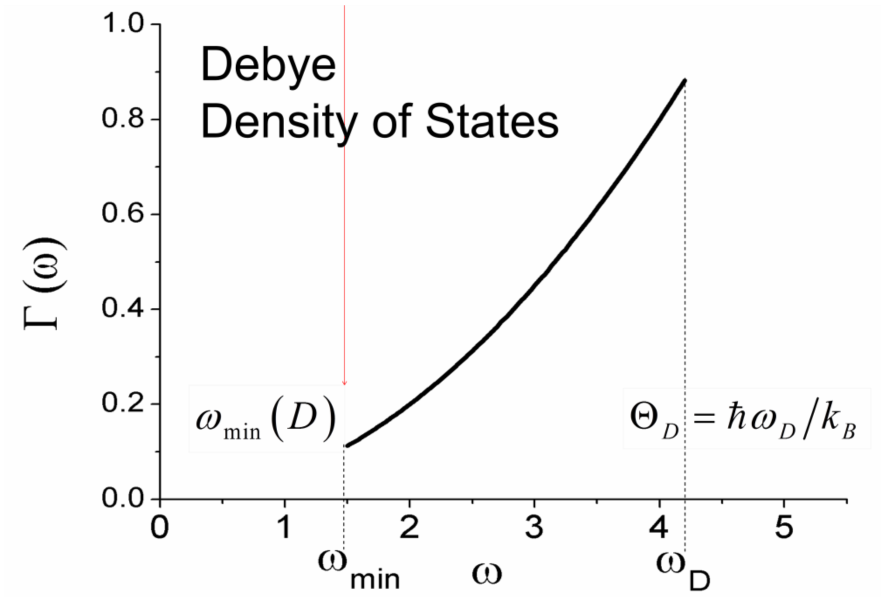

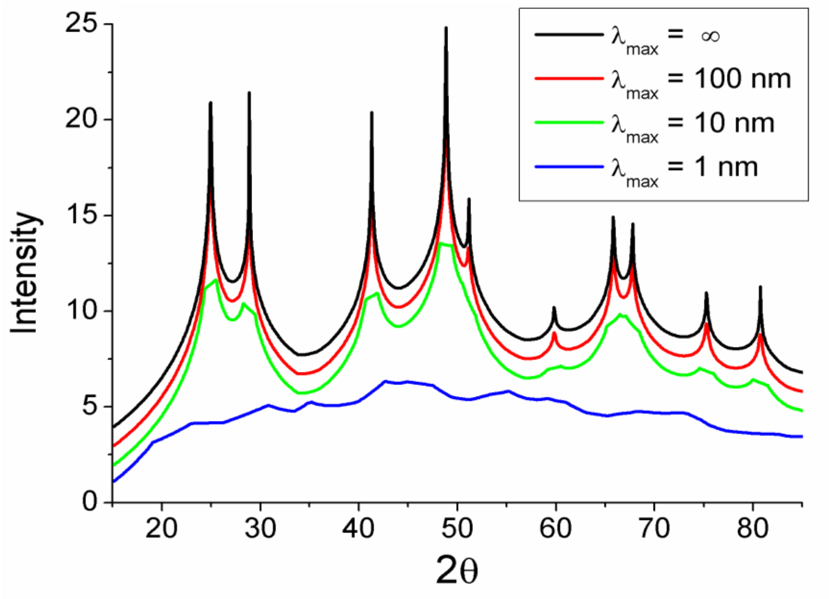

DIFFRACTION FROM NANOCRYSTALLINE *POWDER*

TDS in ball-milled FeMo nanocrystals: static and dynamic contributions

Argonne 11bm, 30keV – 100, 200, 300K

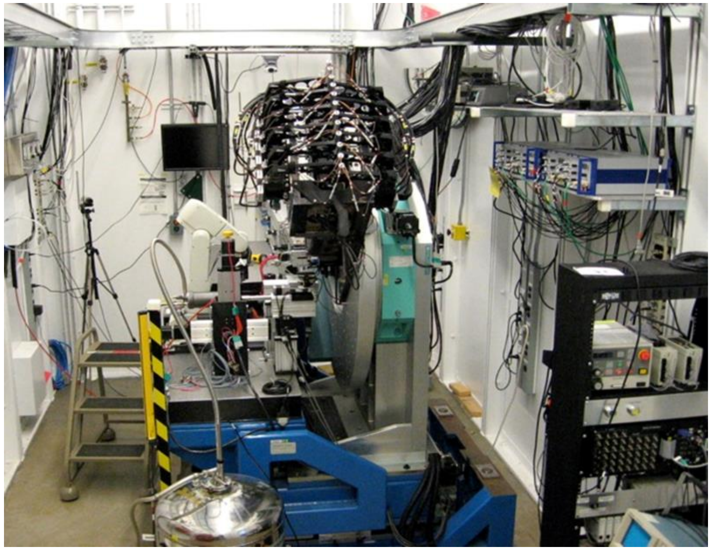

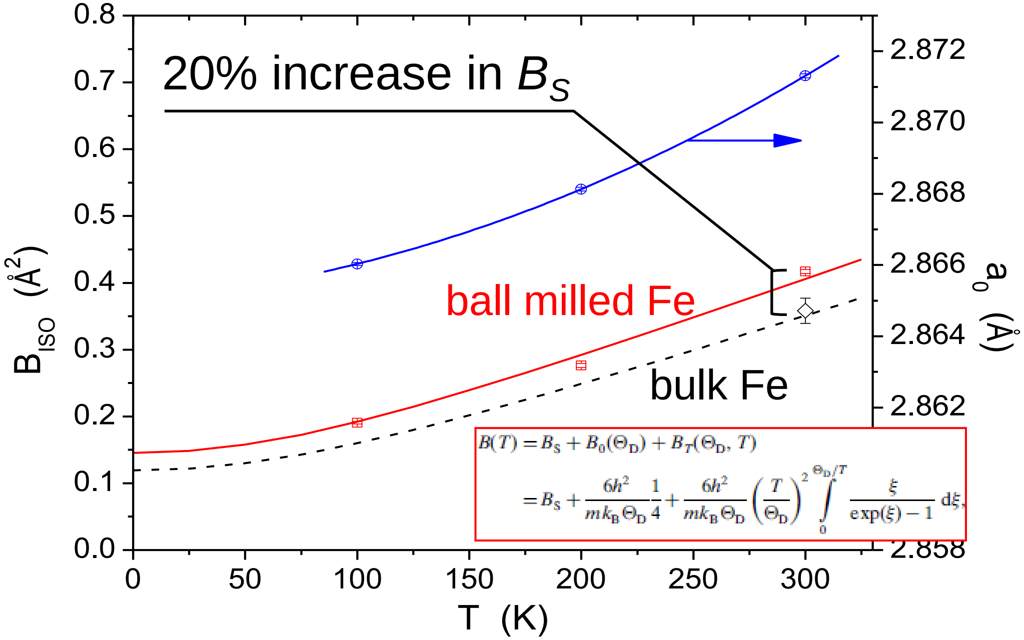

$$B(T) = B_S + B_0(\Theta_D) + B_T(\Theta_D, T)$$
$$= B_S + \frac{6h^2}{mk_B\Theta_D}\frac{1}{4} + \frac{6h^2}{mk_B\Theta_D}\left(\frac{T}{\Theta_D}\right)^2 \int_0^{\Theta_D/T} \frac{\xi}{\exp(\xi)-1}\,d\xi,$$

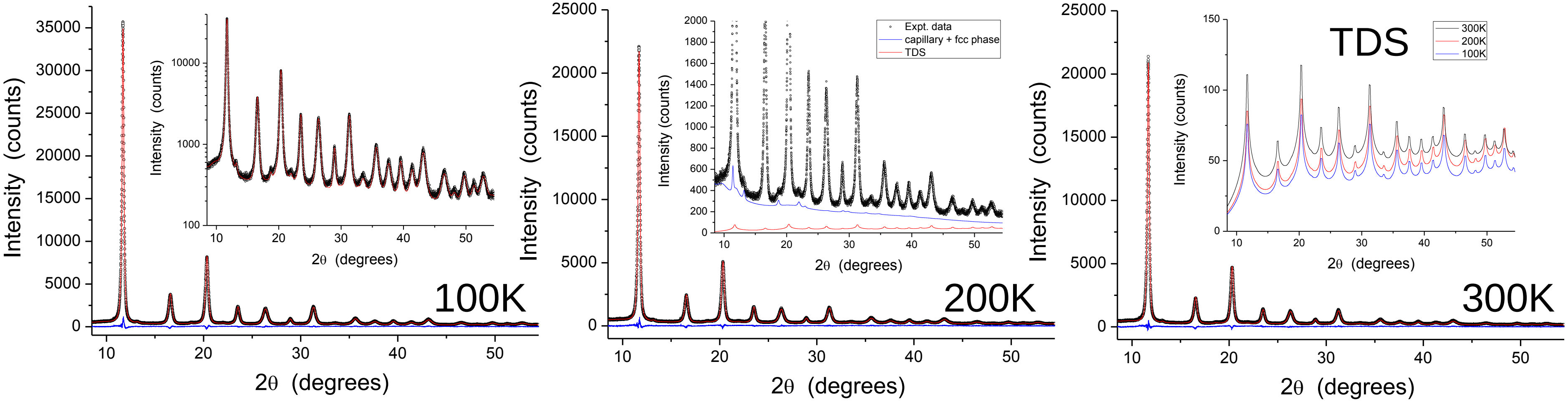

ICTP School - Trieste, 10.05.2018

P. Scardi et al. J. Appl. Cryst. 50 (2017) 508

DIFFRACTION FROM NANOCRYSTALLINE *POWDER*

EXAFS & XRD : Mean Square Displacement (MSRD, MSD) and DCF

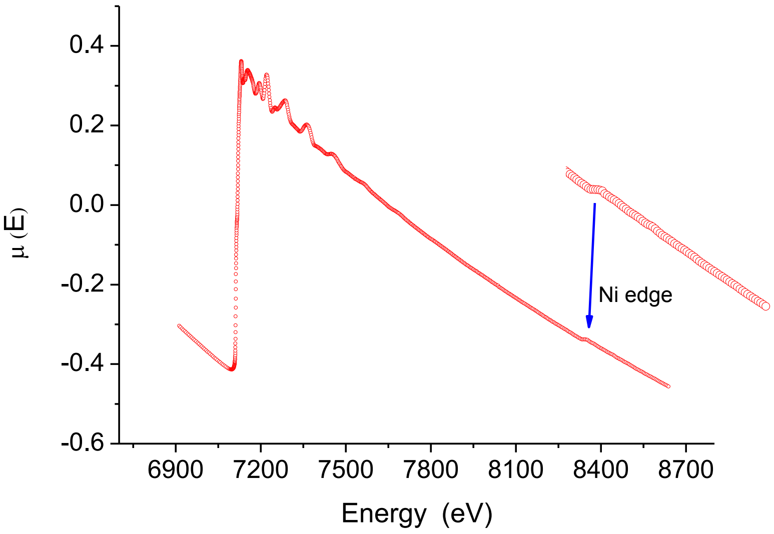

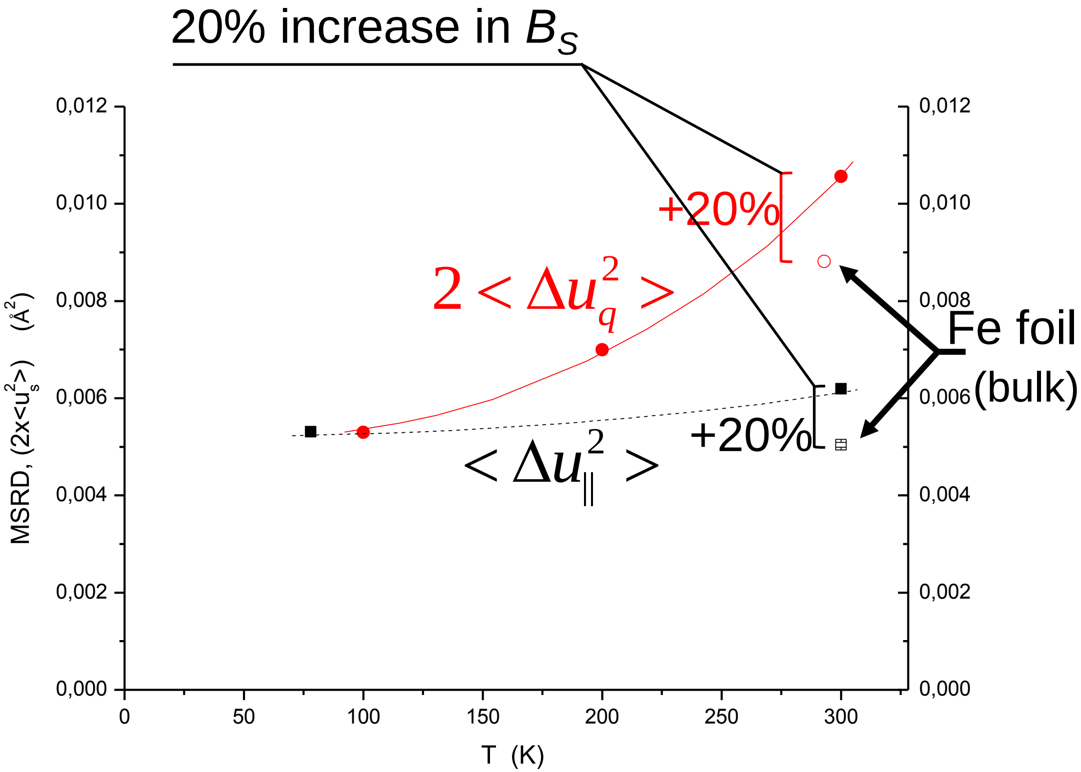

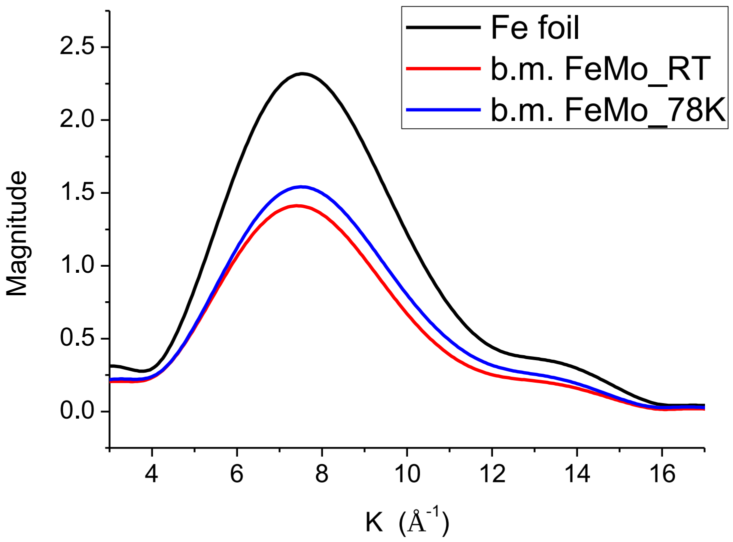

- EXAFS Debye-Waller parm. $< \Delta u_{\parallel}^2 >$: 1° coordination shell
- XRD Debye-Waller parm. $< \Delta u_q^2 >= B/8\pi^2$: average over whole crystal

$$< \Delta u_{\parallel}^2 >= MSRD = 2 \times < \Delta u_q^2 > - DCF$$

P. Scardi et al. J. Appl. Cryst. 50 (2017) 508

DIFFRACTION FROM NANOCRYSTALLINE *POWDER*

What is the main reason for the 20% increase in B_S (static disorder) ?

Molecular Dynamics simulation of a cluster of 50 Fe grains (size distribution from XRD/WPPM)

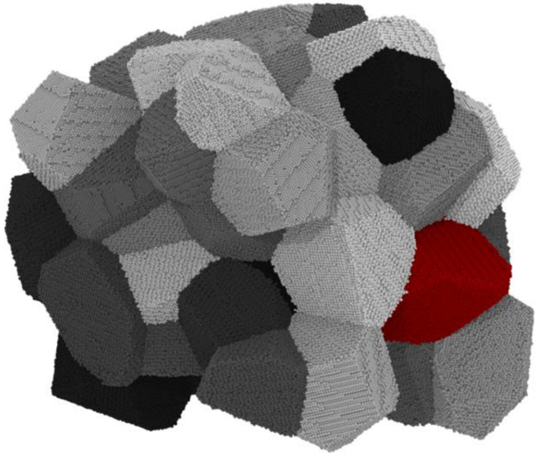

MSD - Mean Square Displacement $< \Delta u_q^2 >$ ($B=8\pi^2 < \Delta u_q^2 >$)
results for average-size grain (G5)

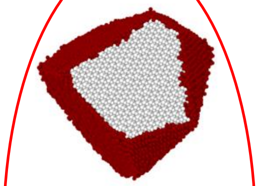

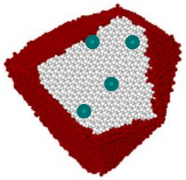

	no defects g.b. only	1 edge disloc. and g.b.	vacancies and g.b.
$\Delta B = B_{G5} - B_{bulk}$	22%	22%+ ~2%	22%+ ~0% (<<1%)

P. Scardi et al. J. Appl. Cryst. 50 (2017) 508

FROM SINGLE CRYSTAL TO POWDER DIFFRACTION

Traditional reciprocal space approach : sum & average

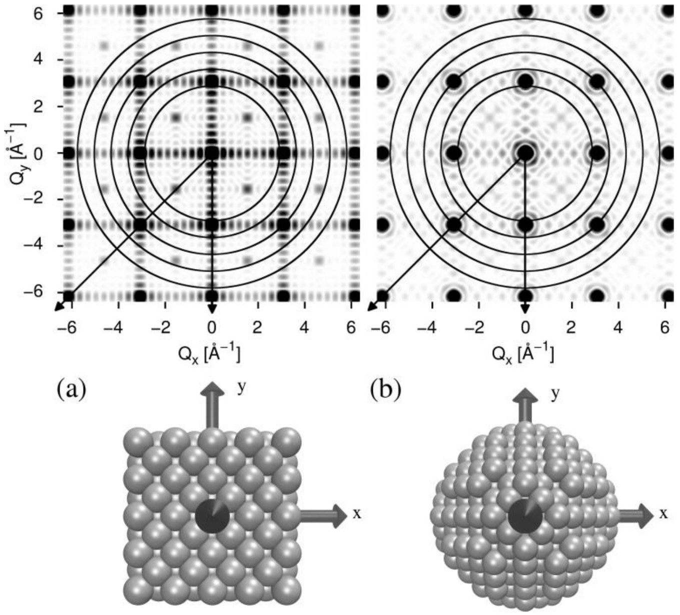

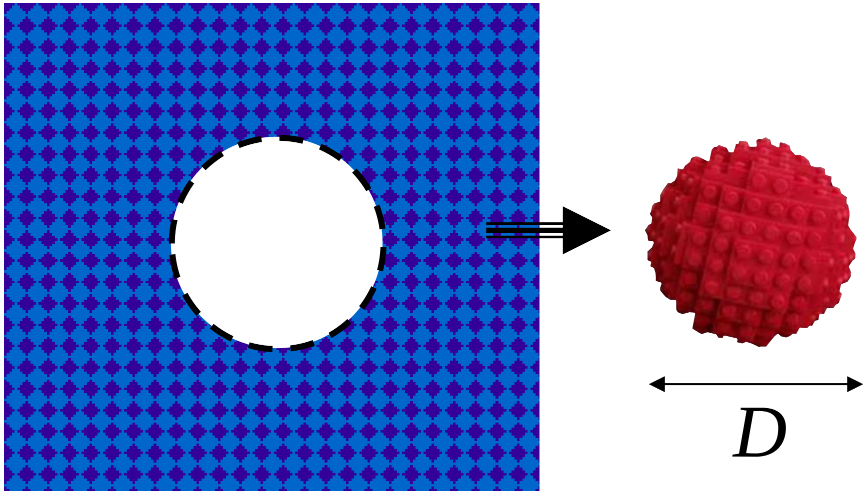

perfect (infinite) crystal

$$I_{sc}\left(\underline{s}\right) \propto \sum_{m}\sum_{n} f_m f_n^{*} e^{2\pi i\left(\underline{S}\cdot\underline{r}_{mn}\right)}$$

$$I_{PD}\left(s\right) \propto \frac{\int I_{sc}\left(\underline{s}\right) d\Omega}{4\pi s^{2}} = \left|F\right|^{2} \cdot \left\{I^{IP}\left(s\right)\otimes I^{S}\left(s\right)\otimes I^{D}\left(s\right)\otimes I^{F}\left(s\right)\otimes I^{APB}\left(s\right)\otimes I^{C}\left(s\right)\otimes I^{GSR}\left(s\right)\ldots\right\}$$

PRESENTATION OUTLINE

PART II May 10, 17:00 – 18:30

- Computer lab:
  hands-on session with TOPAS

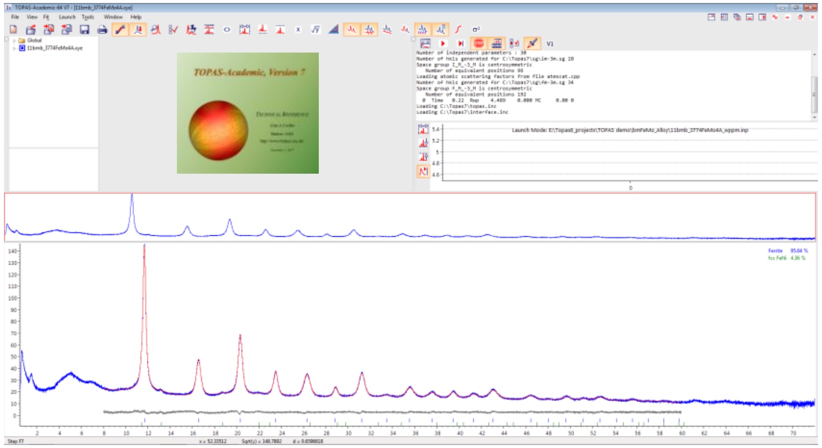

```
Number of independent parameters : 38
Number of hkls generated for C:\Topas7\sg\im-3m.sg 28
Space group I_M_-3_M is centrosymmetric
  Number of equivalent positions 96
Loading atomic scattering factors from file atmscat.cpp
Number of hkls generated for C:\Topas7\sg\fm-3m.sg 34
Space group F_M_-3_M is centrosymmetric
  Number of equivalent positions 192
 0  Time   0.22  Rwp    4.489    0.000 MC     0.00 0
Loading C:\Topas7\topas.inc
Loading C:\Topas7\interface.inc
```

Launch Mode: E:\Topas6_projects\TOPAS demo\bmFeMo_Alloy\11bmb_3774FeMo4A_wppm.inp

x = 52.33512   Sqrt(y) = 148.7892   d = 0.6596618

DIFFRACTION FROM NANOCRYSTALLINE MATERIALS

☹ real nanocrystals are complex objects

non-crystallographic (e.g. multiply twinned) nanoparticles, 2D and highly disordered layer systems:

- translational symmetry: not verified
- large strain / misfit – complex local atomic arrangement

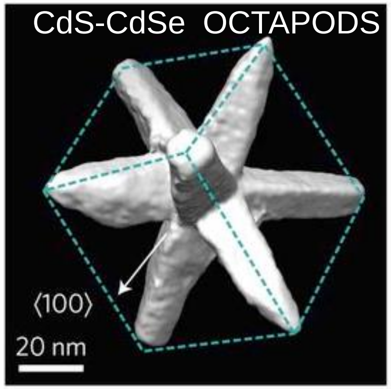

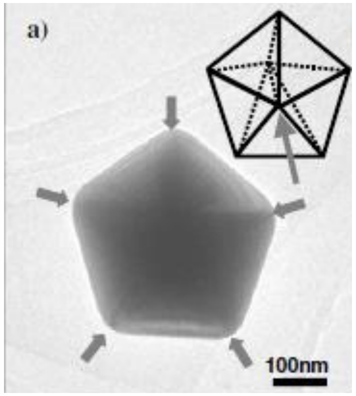

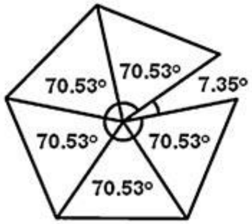

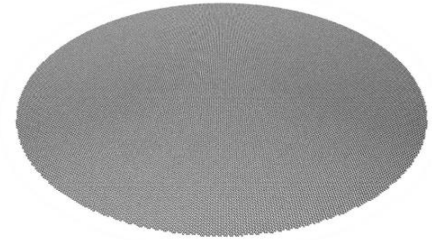

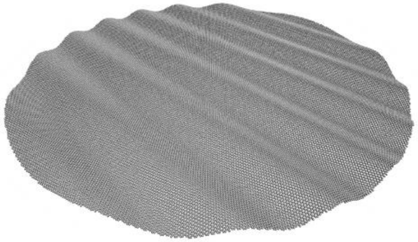

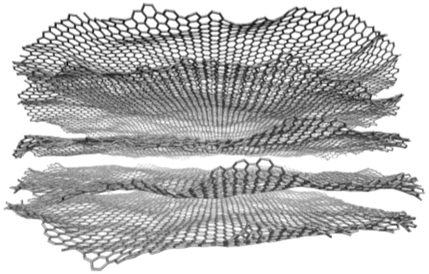

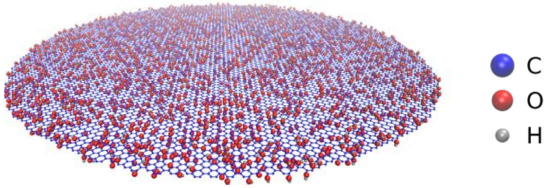

DIFFRACTION FROM NANOCRYSTALLINE MATERIALS

Direct (real) space approach : average & sum

$$I_{PD}(s) = \frac{\int \sum_m \sum_n f_m f_n^* e^{2\pi i(\underline{s} \cdot \underline{r}_{mn})} d\Omega}{4\pi s^2}$$

DIFFRACTION FROM NANOCRYSTALLINE MATERIALS

Direct (real) space approach : average & sum

$$I_{PD}(s)=\frac{|f|^2\sum_m\sum_n\underbrace{\int e^{2\pi i(\underline{s}\cdot\underline{r}_{mn})}d\Omega}_{}}{4\pi s^2}$$

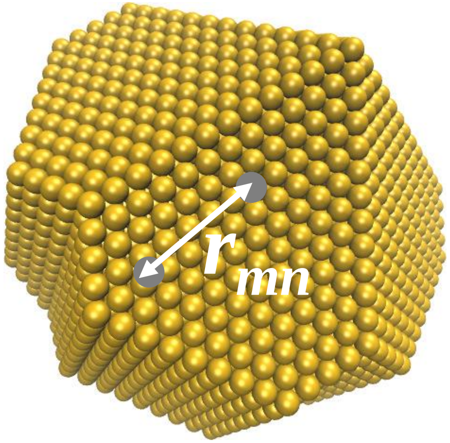

$$\left\langle e^{2\pi i(\underline{s}\cdot\underline{r}_{mn})}\right\rangle=\frac{1}{4\pi r_{mn}^2}\int_0^\pi e^{2\pi i s r_{mn}\cos\phi}\,2\pi r_{mn}^2\sin\phi\, d\phi=\frac{\sin(2\pi s r_{mn})}{2\pi s r_{mn}}$$

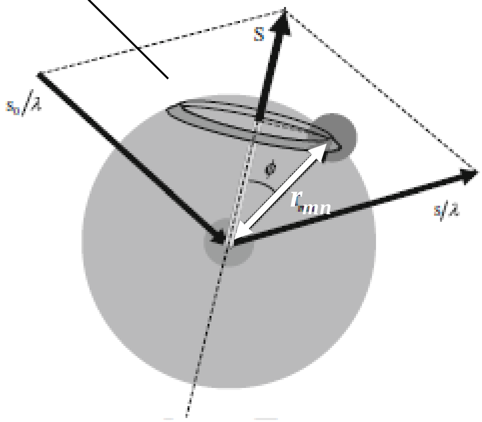

$$I_{PD}(s)=|f|^2\sum_m\sum_n\frac{\sin(2\pi s r_{mn})}{2\pi s r_{mn}}$$

Debye Scattering Equation (DSE)

DSE APPLICATION TO NON-CRYSTALLOGRAPHIC NPs

Debye Scattering Equation (DSE)

$$I_{PD}(s) = |f|^2 \sum_m \sum_n \frac{\sin(2\pi s r_{mn})}{2\pi s r_{mn}}$$

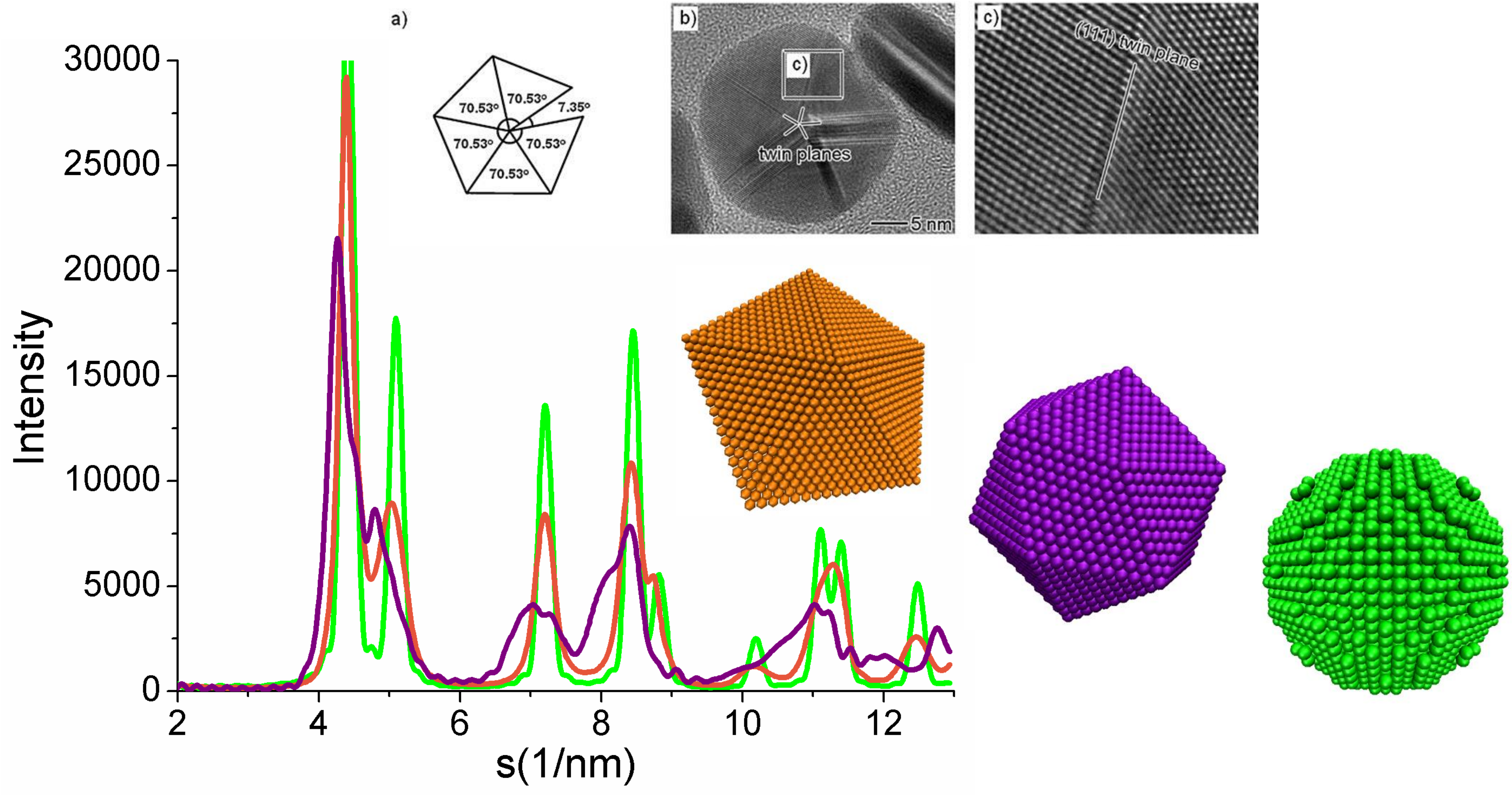

DSE APPLICATION TO GRAPHENE AND RELATED MATERIALS

Debye Scattering Equation (DSE)

$$I_{PD}(s) = |f|^2 \sum_m \sum_n \frac{\sin(2\pi s r_{mn})}{2\pi s r_{mn}}$$

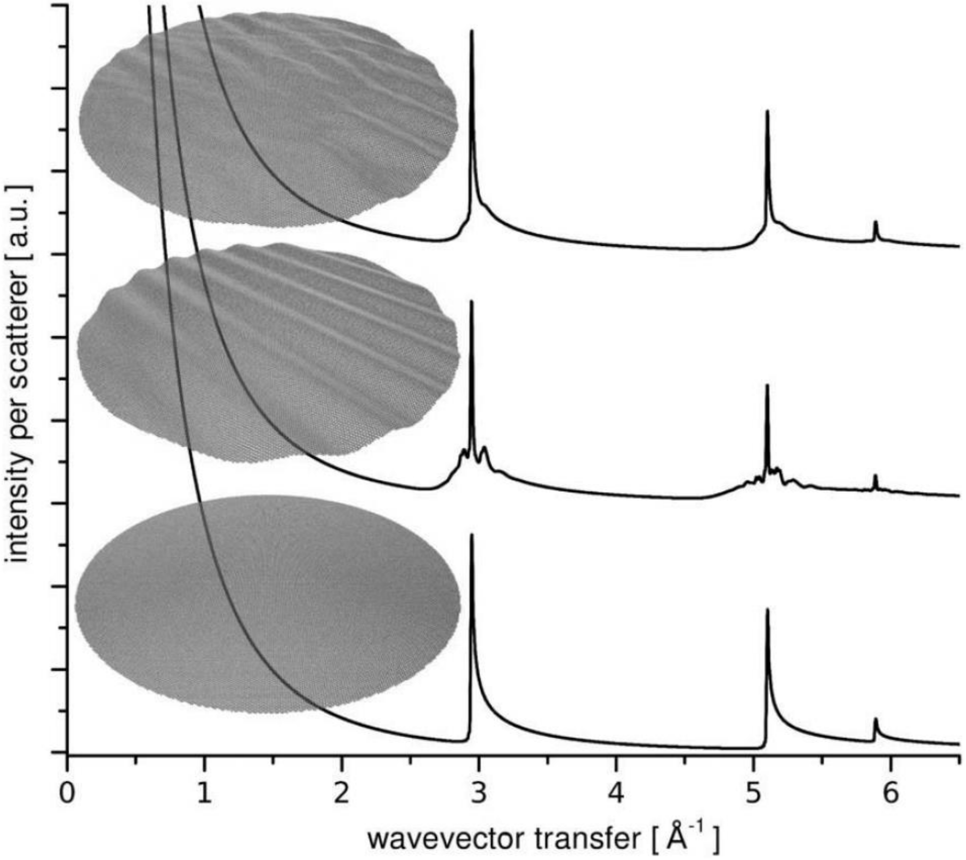

Figure 7
Powder patterns for graphene disks of diameter D = 500 Å. Regular, flat graphene (bottom), undulate graphene (middle) and graphene with a random roughness (top). See text for details.

L. Gelisio et al., J. Appl. Cryst. 43 (2014) 647

DSE APPLICATION TO GRAPHENE AND RELATED MATERIALS

Debye Scattering Equation (DSE)

$$I_{PD}(s) = |f|^2 \sum_m \sum_n \frac{\sin(2\pi s r_{mn})}{2\pi s r_{mn}}$$

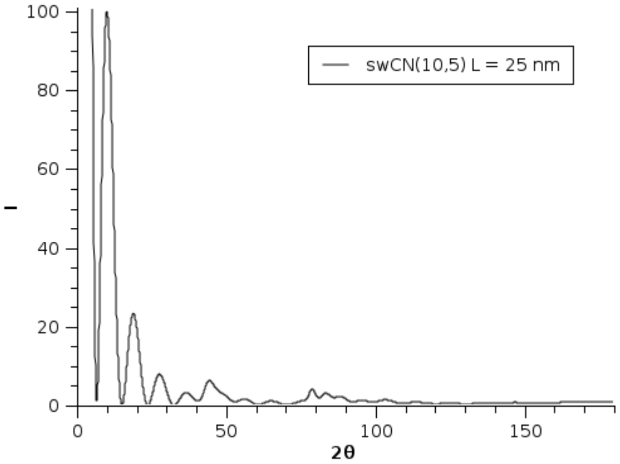

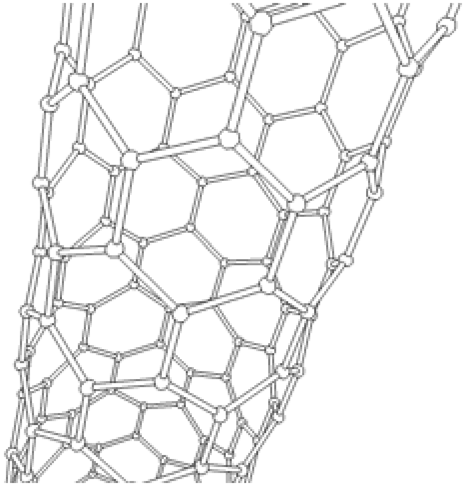

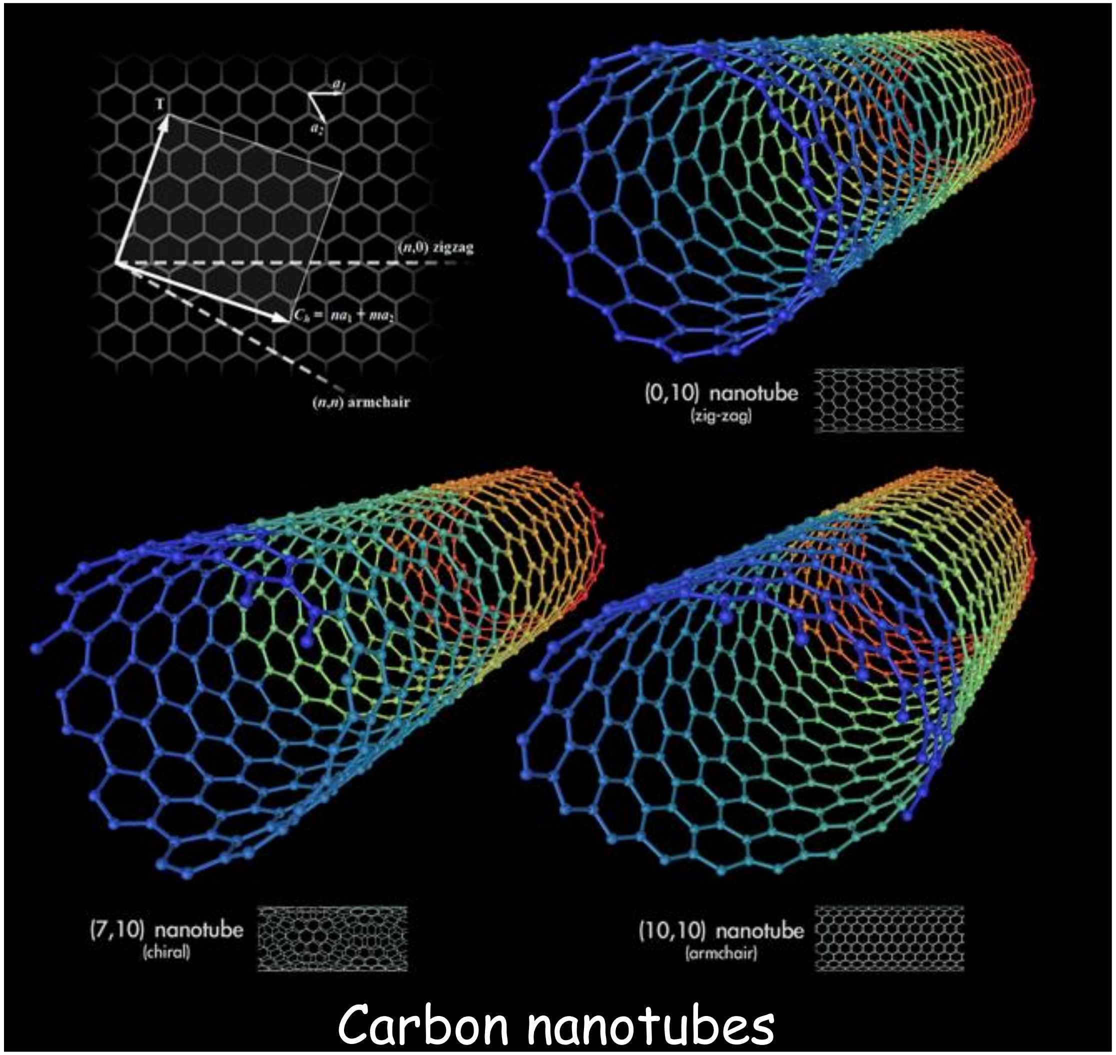

Carbon nanotubes

GENERAL REFERENCES

B.E. Warren, *X-ray Diffraction*, Addison-Wesley, Reading, MA, 1969.

A. Guinier, *X-ray Diffraction*, Freeman & Co, S. Francisco, 1963.

A.J.C. Wilson, *X-ray Optics*, 2nd ed., Methuen & Co, London, 1962.

H.P. Klug & L.E. Alexander, *X-ray Diffraction procedures*, Wiley, New York, 1974.

B.D. Cullity, *Elements of X-ray Diffraction*, Addison-Wesley, Reading Ma, 1978.

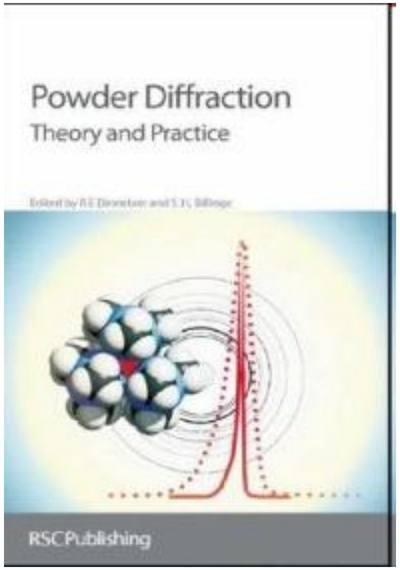

Powder Diffraction
Theory and Practice

RSC Publishing

Powder Diffraction: Theory and Practice

R.E. Dinnebier & S.J.L. Billinge, editors.

Cambridge: Royal Society of Chemistry, 2008.

P. Scardi, Chapter 13 on Line Profile Analysis:

REFERENCES - Paolo.Scardi@unitn.it

Extending the Reach of Powder Diffraction Modelling by User Defined Macros
P. Scardi & R. E. Dinnebier, editors
A special issue of Materials Science Forum, 2010.

Diffraction Analysis of Materials Microstructure
E.J. Mittemeijer & P. Scardi, editors.
Berlin: Springer-Verlag, 2004.

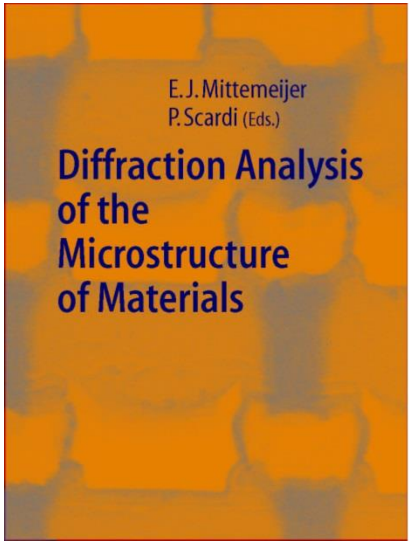
E.J. Mittemeijer
P. Scardi (Eds.)
Diffraction Analysis of the Microstructure of Materials

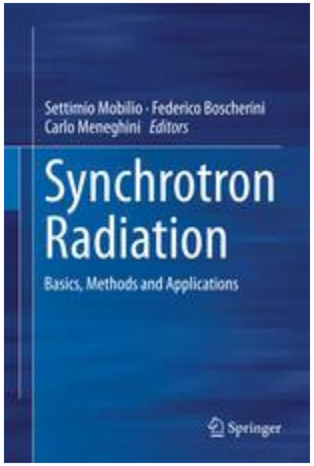
Settimio Mobilio · Federico Boscherini
Carlo Meneghini Editors
Synchrotron Radiation
Basics, Methods and Applications
Springer

Synchrotron Radiation.
Basics, Methods and Applications
S. Mobilio, F. Boscherini, C. Meneghini, editors.
Springer-Verlag, 2015